NEUROSCIENCE
RESEARCH ARTICLE
A. L. Mendell et al. / Neuroscience 429 (2020) 185–202

Inhibition of 5α Reductase Impairs Cognitive Performance, Alters Dendritic Morphology and Increases Tau Phosphorylation in the Hippocampus of Male 3xTg-AD Mice

Ari Loren Mendell,[a] Samantha D. Creighton,[b] Hayley A. Wilson,[a] Kristen H. Jardine,[b] Lauren Isaacs,[a] Boyer D. Winters[b] and Neil J. MacLusky[a]*

[a] Departments of Biomedical Sciences, N1G 2W1, Canada

[b] Psychology, University of Guelph, Guelph, Ontario, N1G 2W1, Canada

Abstract—Recent work has suggested that 5α-reduced metabolites of testosterone may contribute to the neuroprotection conferred by their parent androgen, as well as to sex differences in the incidence and progression of Alzheimer's disease (AD). This study investigated the effects of inhibiting 5α-reductase on object recognition memory (ORM), hippocampal dendritic morphology and proteins involved in AD pathology, in male 3xTg-AD mice. Male 6-month old wild-type or 3xTg-AD mice received daily injections of finasteride (50 mg/kg i.p.) or vehicle (18% β-cyclodextrin, 1% v/b.w.) for 20 days. Female wild-type and 3xTg-AD mice received only the vehicle. Finasteride treatment differentially impaired ORM in males after short-term (3xTg-AD only) or long-term (3xTg-AD and wild-type) retention delays. Dendritic spine density and dendritic branching of pyramidal neurons in the CA3 hippocampal subfield were significantly lower in 3xTg-AD females than in males. Finasteride reduced CA3 dendritic branching and spine density in 3xTg-AD males, to within the range observed in vehicle-treated females. In the CA1 hippocampal subfield, dendritic branching and spine density were reduced in both male and female 3xTg-AD mice, compared to wild type controls. Hippocampal amyloid β levels were substantially higher in 3xTg-AD females compared to both vehicle and finasteride-treated 3xTg-AD males. Site-specific Tau phosphorylation was higher in 3xTg-AD mice compared to sex-matched wild-type controls, increasing slightly after finasteride treatment. These results suggest that 5α-reduced neurosteroids may play a role in testosterone-mediated neuroprotection and may contribute to sex differences in the development and severity of AD.

Key words: hippocampus, Alzheimer, mouse, tau phosphorylation, dendritic structure.

INTRODUCTION

Gonadal steroid hormone levels decline with age in both sexes, a change that has been associated with age-related increases in the risk for development of Alzheimer's disease (AD). AD is approximately twice as likely to develop in women, a sex difference that has been related to the abrupt decline in circulating ovarian steroid hormone levels occurring at menopause (Seshadri et al., 1997; Plassman et al., 2011; Hebert et al., 2013; Alzheimer's Association, 2014; Hanamsagar and Bilbo, 2016). Although the decline in testosterone levels in men is more gradual, it has also been proposed to represent a risk factor for the development of AD (Hogervorst et al., 2001, 2003, 2004; Yeap et al., 2008; Hsu et al., 2015).

In mouse models of AD, several groups have demonstrated that testosterone is neuroprotective, in both sexes. In the triple transgenic mouse model of AD (3xTg-AD), gonadectomy (GDX) has been reported to increase accumulation of amyloid β (Aβ), impair working memory, increase anxiety, and slightly increase hyperphosphorylation of Tau (Rosario et al., 2006, 2010; , 2012; George et al., 2013). Long-term replacement with testosterone or its androgenic 5α-reduced metabolite dihydrotestosterone (DHT) has been shown to prevent these outcomes in males (Rosario et al., 2006, 2010, 2012). In females, the effects of testosterone are at least partially mediated via local aromatization to estradiol (MacLusky et al., 2006), which exerts its effect

*Corresponding author. Address: Department of Biomedical Sciences, Ontario Veterinary College, University of Guelph, Guelph, Ontario N1G 2W1, Canada.
E-mail address: nmaclusk@uoguelph.ca (N. J. MacLusky).

Abbreviations: AD, Alzheimer's disease; AEBSF, 4-(2-aminoethyl)-benzenesulfonyl fluoride; AR, androgen receptor; Aβ, amyloid β; BSA, bovine serum albumin fraction V; DAB, 3,3′-Diaminobenzidine; DHT, dihydrotestosterone; DR, discrimination ratio; ER, estrogen receptors; GABA, γ-aminobutyric acid; GDX, gonadectomy; i.p., intraperitoneal; IHC, immunohistochemistry; KPBS, potassium PBS; ORM, object recognition memory; PB, phosphate buffer; PBS, phosphate-buffered saline; PFA, paraformaldehyde; TBS, tris-buffered saline.

https://doi.org/10.1016/j.neuroscience.2020.01.011
0306-4522/

by interacting with the estrogen receptors (ER) expressed in the brain (Milner et al., 2001, 2005; Adams et al., 2002; Kritzer, 2006; Duarte-Guterman et al., 2015; Mogi et al., 2015). Estradiol has been shown to reduce Aβ levels and reverse memory deficits in female GDX 3xTg-AD mice (Carroll et al., 2007; Zhao et al., 2011), as well as reduce Aβ load in GDX double transgenic (APPswe/PS1) (Zheng et al., 2002) and APPswe transgenic mice (Levin-Allerhand et al., 2002; Zheng et al., 2002). GDX has been reported to increase Aβ levels in the brains of female guinea pigs (Petanceska et al., 2000), and both female and male rats (Ramsden et al., 2003; Jayaraman et al., 2012). These effects were reversed by estradiol and DHT supplementation in females and males, respectively (Petanceska et al., 2000; Ramsden et al., 2003; Jayaraman et al., 2012).

In the male, the neuroprotective effects of testosterone have mainly been attributed to androgen receptor (AR)-mediated effects of testosterone and DHT. However, other bioactive steroids are also synthesized via DHT metabolism. These include the weakly androgenic metabolites 5α-androstane-3α,17β-diol (3α-diol) and 5α-androstane-3β,17β-diol (3β-diol), synthesized by 3α-hydroxysteroid dehydrogenase (3α-HSD) and 3β-hydroxysteroid dehydrogenase (3β-HSD), respectively. As a 3α-hydroxy, 5α-reduced neurosteroid, 3α-diol can act as a positive allosteric modulator of the γ-aminobutyric acid (GABA) A receptor ($GABA_AR$), while 3β-diol is an agonist for ERβ receptors (Handa et al., 2008; Reddy and Jian, 2010).

Although it is one of the principal metabolites of testosterone, in both the brain and in non-neural androgen target organs, relatively few studies have evaluated the behavioral and neuroprotective effects of 3α-diol. Long-term systemic administration or acute intrahippocampal infusion of 3α-diol or its androgenic precursors increased learning and reduced anxiety in GDX male rats (Edinger and Frye, 2004). More recently, the same group has reported that 3α-diol can increase performance on tasks evaluating cognitive function and affective behaviour in young GDX as well as older intact male rats (Frye et al., 2010). Several studies have recently demonstrated that 3α-diol can protect neurons and neuroblastoma cells against neurotoxicity induced by Aβ *in vitro*, by attenuating the Aβ-mediated dysregulation of signaling pathways (Mendell et al., 2016, 2018) as well as improving aspects of mitochondrial bioenergetics (Grimm et al., 2014, 2016).

The present study was performed to test the hypothesis that inhibition of 5α-reductase, the rate-limiting enzyme in the synthesis of both DHT and 3α-diol from testosterone, might result in impairments of hippocampal-based memory, alter hippocampal neuronal dendritic structure and affect markers of pathology in male 3xTg-AD mice.

EXPERIMENTAL PROCEDURES

Animals

Colonies of wild-type (B6129SF2/J; The Jackson Laboratory, Bar Harbor, ME, USA) and 3xTg-AD (B6129APPswe, PS1M146V, TauP301L; The Jackson Laboratory) mice were housed and bred at the University of Guelph Central Animal Facility. All mice used in this study were bred in-house and maintained on a 12-hour light/dark cycle (0800 lights on; 2000 h lights off) Mice were housed in polyethylene cages (16 × 12 × 26 cm) with corncob bedding, crink-l'Nest and cotton nest squares and food (Teklad Global 16% Protein Rodent Maintenance Diet, Harlan Teklad, USA) and water available *ad libitum*. All procedures involving the use of animals were approved by the Animal Care Committee of the University of Guelph and followed the guidelines of the Canadian Council of Animal Care.

A total of 55 mice (10 wild type females, 17 wild type males, 9 3xTg-AD females and 19 3xTg males) were used in this study. At six months of age, mice began receiving daily intraperitoneal (i.p.) injections of either vehicle [18% w/v 2-hydroxypropyl-β-cyclodextrin (Sigma-Aldrich, Oakville, ON, Canada) in 0.9% saline solution; β-CD solution] or finasteride [50 mg/kg in β-CD solution; a dose that substantially reduces peripheral and CNS 5α reduced steroid concentrations with both acute and chronic use (Finn et al., 2006)]. Mice were weighed immediately prior to each daily injection and injection volumes were adjusted to 1% of the body weight (v/b.w.). Male wild-type and 3xTg-AD mice received either vehicle (denoted wtm-V and 3xm-V, respectively) or finasteride (denoted wtm-F and 3xm-F, respectively) injections (n = 8–10 mice/group); female wild-type and 3xTg-AD mice received vehicle injections only (n = 9–10 mice/group; denoted wtf-V and 3xf-V, respectively).

Habituation for behavioural testing occurred on days 15 and 16 of injections, behavioural testing was performed on days 17 and 19, and animals were sacrificed 2 hours following the final finasteride or vehicle injection on day 20. Approximately half the mice in each treatment group were sacrificed by deep anesthetization with carbon dioxide (CO_2) followed by decapitation (the numbers in each group are indicted below, in the Results section). The remainder were sacrificed by Euthansol (Schering Canada Inc., Quebec) injection followed by transcardial perfusion with 4% paraformaldehyde (PFA), for immunohistochemical analysis.

For all animals that were sacrificed by CO_2 and decapitation, brains were extracted, placed on ice, and cut in half down the longitudinal fissure using a sterile razor blade. One half of each brain was placed directly into fresh Golgi-Cox solution for neuromorphological analysis. The hippocampus was dissected out of the other half of each brain, and these tissue samples were placed on dry ice prior to immediate storage at −80 °C. The samples from each treatment group included approximately equal numbers from the left and right sides of the brain, to minimize the effects of lateralization as a factor in the final analysis.

Object recognition memory task

The object recognition memory (ORM) task was performed in an open field made of white corrugated plastic with dimensions of 45 cm (length) × 45 cm

(width) × 30 cm (height). Spatial cues throughout the testing room were readily available and additional cues were placed on the walls around the open field apparatus. Animals were habituated to the open field for 10-minute periods on each of the two days prior to commencing behavioural testing. During these habituation periods, all conditions of the room were set up in an identical way as testing days with the exception that no objects were placed in the open field. For testing, mice were placed into the centre of the open field with two identical objects in adjacent corners of the apparatus and allowed to explore for 10 minutes (sample phase). Objects were chosen based on preliminary trials with wild type mice, demonstrating that the animals had no inherent preference for the objects chosen. At the end of the sample phase, mice were removed from the open field and placed back into their home cages for either 5 minutes or 3 hours (retention delay) to assess short- and long-term memory, respectively. After the retention delay, mice were placed back into the centre of the open field apparatus with one object that the animal had previously been exposed to during the sample phase (familiar) and one new object (novel), and provided 5 minutes to explore the two objects (choice phase) (task design illustrated in Fig. 1 A). The two objects were located in the same positions as in the sample phase. Which object was novel and which familiar was counterbalanced in each set of analyses, so that it is not always one particular type of object that was novel. The side of the test cage (left or right) on which the novel object was placed was also counterbalanced in the choice phase of the test, to prevent preference for one side or the other from influencing the results. All mice were run for each of the two retention delays on separate days, with one day of rest between testing days. All objects were thoroughly wiped with 70% ethanol between trials to reduce the influence of olfactory cues.

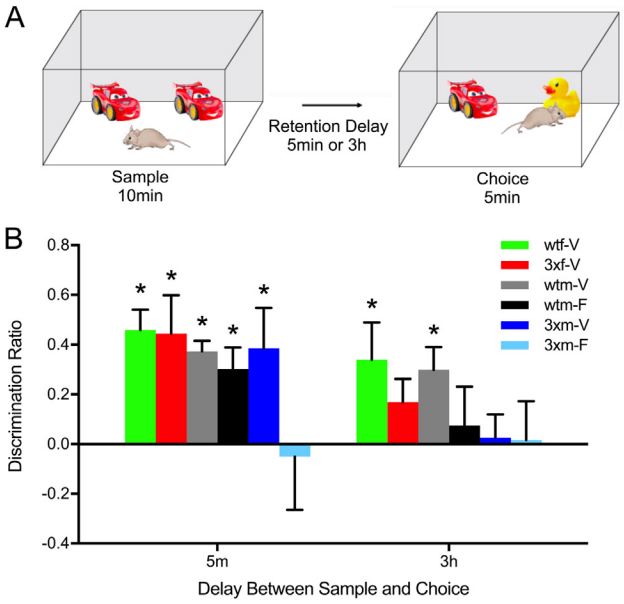

Fig. 1. Object recognition memory (ORM) in wild-type and 3xTg-AD mice. **(A)** Schematic for the ORM paradigm in the open field. **(B)** Finasteride treatment impairs short-term (5 minute delay) ORM in male 3xTg-AD mice, while long-term (3 hour delay) ORM is impaired in all 3xTg-AD mice and in finasteride-treated male wild-type mice **(B)**. Bars on the graph represent mean ± SEM (n = 7–10 mice/group). Group acronyms: wtf-V = wild-type females treated with vehicle; 3xf-V = 3xTg-AD females treated with vehicle; wtm-V = wild-type males treated with vehicle; wtm-F = wild-type males treated with finasteride; 3xm-V = 3xTg-AD males treated with vehicle; 3xm-F = 3xTg-AD males treated with finasteride. * = $p < 0.05$ vs. a DR of zero (Student's t test).

Due to the natural novelty preference of mice, they explore familiar objects less than novel objects (Ennaceur and Delacour, 1988). If the animals have memory impairments, they are less able to discriminate between the familiar and novel objects. A discrimination ratio (DR) was used to calculate novelty preference for each subject [DR = (exploration time of novel object – exploration time of familiar object)/(exploration time of both objects combined)].

Locomotor behavior

Locomotion of each mouse was tracked in the first sample phase of the open-field object recognition task in order to examine anxiety-like behaviours. EthoVision XT video tracking software was employed to collect the locomotor data. A square centre zone (22.5 cm × 22.5 cm) and a periphery zone were outlined in the arena on the video tracking software. The distance moved (cm) and time spent (s) within each zone was recorded. We assessed two measures of anxiety-like behaviour based on the locomotor activity; (1) percentage of time spent in the centre zone compared to total time in the arena (10-min), and (2) total distance moved.

Tissue preparation for neuromorphological analysis

Golgi-Cox solution was prepared as previously described (Louth et al., 2017). Half brains from a subset of the mice used in this study (n = 5–6 mice/group) were stored in Golgi-Cox solution in the dark at room temperature for 25 days. After the incubation period, samples were placed in 30% sucrose solution in 0.1 M phosphate buffer (PB) for 48 hours at 4 °C. Samples were then blocked in 3% agar (Fisher), vibratome-sectioned in the coronal plane (300 μm thickness) using a Leica VT1000S vibrating blade microtome (Leica Biosystems, Concord, ON, Canada) in 30% sucrose solution, and placed in 6% sucrose solution at 4 °C for 24 hours. Sections were processed, mounted onto gelatin-coated microscope slides, dehydrated in ethanol, cleared in xylene, and cover-slipped as previously described (Louth et al., 2017). Slides were left horizontally to dry overnight and sealed by painting the edges with clear nail polish the following day.

Analysis of dendritic structure

Dendritic branching analysis. Image stacks were taken for the CA1 and CA3 hippocampal subfields throughout the entire thickness of the vibratome

sections (images captured every 2 μm) of Golgi-stained sections containing the dorsal hippocampus for each animal, using a Nikon Eclipse 90i microscope and motorized stage (Nikon Instruments Inc., Melville, NY, USA) with affixed MBF Bioscience Q-imaging camera (MBF Bioscience, Williston, VT, USA) and Neurolucida software (Version 11, MBF Bioscience). Pyramidal neurons were selected from CA1 and CA3 (3–4 neurons/animal from each subfield, $n = 5–6$ animals/group) and were three-dimensionally traced in Neurolucida. To be included for tracing and analysis, neurons had to be completely contained within the 300 μm-thick section with no broken segments from the cell body out to the end of the dendritic trees (Mendell et al., 2017). Sholl analysis (Sholl, 1953) was performed using Neurolucida Explorer software (MBF Bioscience), with measurements for intersections between dendritic branches and concentric circles taken every 20 μm, starting at the cell body. Apical and basal dendritic arbours were analyzed separately.

Dendritic spine analysis. Images were obtained for dendritic spine density as previously described (Mendell et al., 2017). Sections containing the dorsal hippocampus were examined under brightfield microscopy at high magnification (630X) using an Axio Imager D1 microscope (Carl Zeiss, Toronto, ON, Canada). Pyramidal neurons from the CA1 and CA3 subfields were chosen for dendritic spine imaging and analysis as previously described (Mendell et al., 2017). Images containing secondary dendrites within each of three segments of the apical dendritic tree were captured [proximal (10–30% out from the cell body), medial (40–60%), and distal (70–90%)]. Five to ten images were taken within each apical CA1 and CA3 dendritic segment, for each animal. Images were analyzed using ImageJ (NIH), and dendritic spine density was calculated as the average number of spines per 10 μm length of dendrite. Results were averaged to give a mean spine density per dendrite segment, in each animal. Results were compiled from 4-6 animals/treatment group, to give the final estimates of spine density.

Western blot analysis. Hippocampal tissue samples were homogenized in Triton-X protein lysis buffer [50 mM Tris-HCL (pH 7.5), 150 mM NaCl, 1% Triton-X 100] with added protease inhibitors [(1 mM 4-(2-aminoethyl)-benzenesulfonyl fluoride (AEBSF), 10 μM leupeptin, 10 μM pepstatin A, 25 μM aprotinin)], 700 U/ml DNase, and the phosphatase inhibitor sodium orthovanadate (5 μM). Homogenates were briefly sonicated on a low setting, placed on ice for 20 minutes, and centrifuged twice at 17,530×g for 15 minutes at 4 °C with the supernatants removed and placed in fresh tubes between each centrifuge step. The final pellets were discarded, and protein concentrations were determined for the resulting lysates using Bradford assays (Bradford, 1976). All samples were separated into small aliquots and stored at −20 °C without undergoing any freeze–thaw cycles until the time of analysis.

Western blot analysis was completed as previously described (Mendell et al., 2018). Briefly, hippocampal lysates (25–75 μg of total protein, depending on the target) were loaded onto 10% polyacrylamide gels and subjected to SDS-PAGE using the Mini-PROTEAN system (Bio-Rad, Mississauga, ON, Canada). Proteins were transferred onto nitrocellulose membranes by semi-dry transfer with a Trans-SD Turbo transfer apparatus (Bio-Rad). Transfer conditions included 10–30 minute transfers (depending on target size – small proteins required shorter transfer times) at 25 V with constant current. After transfer, membranes were briefly rinsed with tris-buffered saline (TBS) with 0.1% Tween-20 (TBS-T), and blocked for 1.5–2 hours in 5% non-fat milk, 5% bovine serum albumin fraction V (BSA), or a combination of both at room temperature on a rocker. Membranes were rinsed twice for 5 minutes in TBS-T, and then placed in primary anti-

Table 1. Primary and secondary antibodies used in this study. The table lists the target antigen, the species and type of antibody (mon- or poly-clonal) the dilution used in the Western blot analyses reported in this paper, along with the manufacturer and product number, if further information on the properties and target specificity of the antibodies is required

Target	Species and Type	Dilution Used for Western Blotting	Manufacturer, Product Number
β-Amyloid	Rabbit monoclonal	1:1000	Cell Signaling Technology, 9888
Phospho-Tau Ser202	Rabbit polyclonal	1:1000	Cell Signaling Technology, 11,834
Phospho-Tau Ser396	Mouse monoclonal	1:1000	Cell Signaling Technology, 9632
Tau5 (Total Tau)	Mouse polyclonal	1:1000	BioLegend, 39,413
ERK1/2	Rabbit polyclonal	1:2000	Cell Signaling Technology, 9102
Phospho-ERK1/2	Rabbit polyclonal	1:2000	Cell Signaling Technology, 9101
PSD-95	Mouse monoclonal	1:400	Santa Cruz Biotechnology, Inc., sc32290
NeuN	Rabbit monoclonal	1:1000	Cell Signaling Technology, 24,307
GFAP	Mouse monoclonal	1:5000	Cell Signaling Technology, 3670
17β-HSD type 10 (ERAB)	Rabbit monoclonal	1:500	Abcam, ab167410
3α-HSD type 3 (AKR1C2)	Rabbit polyclonal	1:500	Abcam, ab199608
α-tubulin	Mouse monoclonal	1:200,000	Sigma-Aldrich, T5168
Anti-rabbit IgG, HRP linked antibody	Goat	1:2500	Cell Signaling Technology, 7074
Anti-mouse IgG, HRP linked antibody	Horse	1:2500	Cell Signaling Technology, 7076

body overnight in either 5% non-fat milk or 5% BSA at 4 °C on an orbital shaker (see Table 1 for a list of primary antibodies). The next day, membranes were rinsed twice for 5 minutes in TBS-T and incubated in goat anti-rabbit or goat anti-mouse secondary antibody (1:2500, Cell Signaling Technologies, New England BioLabs, Whitby, ON, Canada) made in 5% non-fat milk or 5% BSA for one hour at room temperature on a rocker. Membranes were then rinsed 4 times for a total of 30 minutes in TBS-T, and bands were visualized using Luminata Forte Western HRP substrate (Millipore Canada Ltd, Etobicoke, ON, Canada) and a ChemiDoc MP imaging system (Bio-Rad). Blots requiring re-probing for house-keeping proteins were rinsed for 4 hours at room temperature in 0.5% TBS-T prior to probing with the primary antibody. Densitometric analysis was performed using Image Lab version 4.1 software (Bio-Rad), with all values for target proteins normalized to a house-keeping protein (α-tubulin) from the same blot.

Immunohistochemistry. A subset of the animals in each treatment group (n = 4–6 per group) was used for immunohistochemistry (IHC). Mice were transcardially perfused with phosphate-buffered saline (PBS) to clear the blood, followed by 4% paraformaldehyde (PFA) for fixation. Brains were dissected out from the skull and post-fixed by immersion in 4% PFA for 36 hours at 4 °C. Brains were then rinsed 3 times with PBS and stored in PBS with 0.1% sodium azide at 4 °C until the time of processing. Brains were blocked in 3% agar, vibratome-sectioned (40 μm thickness) in the coronal plane and the sections placed at 4 °C in PBS with 0.1% sodium azide until IHC analysis.

All processing steps were performed at room temperature with incubations on an orbital shaker. The solvent for all solutions was 0.1 M potassium PBS (KPBS), unless otherwise noted. Sections were rinsed three times with KPBS for 5 minutes each, placed in 0.5% hydrogen peroxide (H_2O_2) for 15 minutes to quench endogenous peroxidase activity and rinsed three times in KPBS. Sections were then placed in 86% formic acid for 5 minutes for antigen unmasking, rinsed three times in KPBS, and incubated in primary antibody solution (0.3% Triton X-100, 10% normal goat serum in KPBS) containing an antibody against Aβ (β-Amyloid [D12B2] Rabbit mAb #9888; 1:1000; Cell Signaling Technology) for 2 hours at room temperature, then overnight at 4 °C. The next day, sections were rinsed three times in KPBS and incubated in secondary antibody solution (0.3% Triton X-100 in KPBS) with biotinylated goat anti-rabbit antibody (1:1000; Cell Signaling Technology) for 1 hour. Sections were then rinsed three times in KPBS and incubated for 1 hour in ABC solution (0.3% Triton X-100, 0.125% avidin, 0.125% biotin in KPBS), rinsed three more times in KPBS, and placed in filtered 3,3′-Diaminobenzidine (DAB) solution (10% DAB, 0.001% H_2O_2 in KPBS) for 7 minutes. Finally, sections were rinsed three times in KPBS, mounted onto gelatin-coated microscope slides, dehydrated in ethanol (50% for 1 minute, 75% for 1 minute, 95% for 1 minute, and 2 steps of 100% ethanol for 5 minutes), cleared in xylene (2 steps for 5 minutes each), and coverslipped using Permount mounting medium (Fisher). Slides were left horizontally to dry overnight and sealed by painting the edges with clear nail polish the following day. All sections used for quantitative comparison were processed at the same time, in the same reagent solutions, in order to minimize between-section variability in background and staining intensity. Controls for immunohistochemistry included primary antibody, secondary antibody and labeling controls (Burry, 2011). Specificity of the primary antibody was demonstrated by coincubation of sections through the same regions of the hippocampus from wild type animals, in the same reagents. Staining was only ever observed in sections from 3xTg mice. Specificity of the secondary antibody was demonstrated by complete loss of staining when the primary antibody incubation was omitted, after formic acid pretreatment. Finally, labeling specificity was demonstrated by a complete absence of staining when the diaminobenzidine incubation was omitted.

Brightfield microscopy images were acquired for subfields of interest at anterior, middle, and posterior levels of the hippocampus (equivalent to dorsal, rostral-ventral, and caudal-ventral hippocampus, respectively) in the anterior-posterior plane of the brain. Quantitative analysis was performed using the NIH ImageJ program, essentially as described by Girish and Vijayalakshmi (2004). Briefly, images were captured for each region of interest, with sections matched as closely as possible in the anterior-posterior plane. Three to four randomly placed, non-overlapping sample fields were taken for analysis of staining intensity, using a constant sized "region of interest" sampling window in all sections, from all animals. A background threshold was set using the ImageJ thresholding tool. Labeling was then assessed as the number of positively stained pixels above the background threshold in each sample window (Girish and Vijayalakshmi, 2004). Results for all sections were averaged to give a mean labeling index per field, for each animal. Results are presented below as means (±SEM) of the average labeling indices in each treatment group.

Statistical analysis. The majority of statistical analyses, with the exception of the analysis of locomotor behavior, were performed using either GraphPad Prism version 7.0 (GraphPad Software Inc., La Jolla, California, USA) or Statview 5.0.1 (SAS Institute, Cary, North Carolina, U.S.). Komolgorov-Smirnov and Bartlett's tests were used to evaluate normality and homogeneity of variance, respectively. Where necessary, data were log(x + 1) transformed prior to statistical analysis to correct for inhomogeneity of variance. Data for the ORM task were analyzed by three-way ANOVA, with unpaired t-tests used to compare individual group means to zero (i.e., 'chance' discrimination ratio). Data for dendritic morphology, western blotting densitometry, and quantitative IHC were analyzed using either ANOVA followed by Tukey-Kramer post-hoc, or Student's t test, as appropriate. Dendritic branching data were analyzed in males using

3-way factorial ANOVA, to test for finasteride treatment-dependent effects. Comparisons between males and females in the dendritic branching results were performed on the data from vehicle treated animals using 3-way ANOVA, followed where significant genotype × sex interactions were observed by separate 2-way ANOVAs in the wild type and 3xTg-AD data sets, to test for genotype specific sex differences. Statistical significance was defined as $p \leq 0.05$.

Differences in locomotor activity between genotype (wildtype, 3xTg-AD) and drug (vehicle, finasteride) conditions were investigated using 2×2 factorial. Independent samples *t*-tests were used to examine differences in locomotion between genotype in the female mice. All analyses of locomotor data used $\alpha = 0.05$ and was analyzed using SPSS 26 Software (IBM, Armonk, NY USA).

RESULTS

Finasteride impaired short-term object recognition memory in male 3xTg-AD mice, while long-term memory was impaired in all 3xTg-AD mice

Short-term (5-minute delay) and long-term (3-hour delay) ORM were evaluated in the open field, as described above, in all 55 mice. Total exploration times were not significantly different between groups in either the sample or choice phases (data not shown). Results are shown in Fig. 1B. Data for the males at each of the two delay times were evaluated by 3-way factorial ANOVA. Significant effects of genotype [$F(1,60) = 4.01$, $p = 0.0498$) and treatment [$F(1,60) = 4.70$, $p = 0.0341$) were observed. Individual *t*-tests were performed to determine whether the animals recognized the change in objects (DR significantly different from zero) or impaired (DR not significantly different from zero) for each treatment group. Short-term ORM was intact, as indicated by significantly greater DRs compared to zero, for all treatment groups (Unpaired Student's *t*-tests; wtf-V, $p < 0.0001$; 3xf-V, $p = 0.0052$; wtm-V, $p < 0.0001$; wtm-F, $p = 0.0011$; 3xm-V, $p = 0.0112$) except for the finasteride-treated male 3xTg-AD group, which had impaired short-term memory (*t*-test; 3xm-F, $p = 0.7964$). For long-term ORM, only the vehicle-treated wild-type female (*t*-test; wtf-V, $p = 0.0364$) and male (*t*-test; wtm-V, $p = 0.0021$) mice had significantly greater DRs compared to 0. All other groups had impaired long-term memory (*t*-tests; 3xf-V, $p = 0.0733$; wtm-F, $p = 0.3892$; 3xm-V, $p = 7880$; 3xm-F, $p = 9158$) (Fig. 1B).

Locomotor behavior

There was no significant interaction between genotype and drug treatment with respect to the time spent in the central zone of the open field arena in the male mice [$F(1,36) = 0.873$, $p = 0.356$], nor for total distance moved in the arena [$F(1,36) = 0.148$, $p = 0.703$]. In females, there was no statistical effect of genotype on time spent in central zone of the open-field arena, $t(18) = -1.890$, $p = 0.075$. However, 3xTG female mice ($M = 5584.50$, SE = 476.05) moved a greater total distance in the arena compared to wildtype female mice ($M = 2150.89$, SE = 238.52), $t(18) = -6.449$, $p < 0.001$).

Dendritic branching

Finasteride reduces dendritic branching in the apical dendrites of CA3 pyramidal neurons in 3xTg-AD mice. Dendritic branching was analyzed separately in the apical and basal dendritic trees of hippocampal pyramidal neurons, in 5–6 animals per treatment group. In males, in the CA3 apical dendritic tree, significant overall treatment [three-way ANOVA; $F(1,464) = 15.68$, $p < 0.0001$], genotype [$F(1,464) = 13.34$; $p = 0.0003$] and distance from cell body-dependent [$F(28,464) = 143.8$, $p < 0.0001$] effects were observed, with a significant genotype × treatment interaction [$F(1,464) = 21.54$, $p < 0.0001$] (Fig. 2 A). Analysis of the data from vehicle treated males and females revealed significant overall effects of sex [$F(1,464) = 10.12$, $p = 0.0016$], genotype [$F(1,464) = 22.27$; $p < 0.0001$] and distance from cell body- [$F(28,464) = 155.9$, $p < 0.0001$], with a significant sex × genotype interaction [$F(1,464) = 32.60$, $p < 0.0001$]. This interaction effect resulted from the reduced dendritic branching observed only in 3xTg-AD females [*F*B; 2-way ANOVA for the female data only: genotype $F(1,232) = 49.27$, $p < 0.0001$; distance from cell body- $F(1,232) = 68.15$, $p < 0.0001$); for males: genotype $F(1,232) = 0.574$, $p = 0.460$; distance from cell body- $F(1,232) = 90.38$, $p < 0.0001$].

In the basal dendritic tree, the only differences observed in males were dependent on the distance from the cell body [$F(13,224) = 260.8$, $p < 0.0001$]. No significant overall treatment [$F(1,224) = 1.01$, $p = 0.315$] or genotype dependent [$F(1,224) = 0.027$, $p = 0.871$] effects were observed. Comparison of males and females in the vehicle treated animals revealed highly significant effects of both distance from the cell body [$F(13,224) = 253.78$, $p < 0.0001$] and sex [$F(1,224) = 15.12$, $p = 0.0001$], but no genotype dependent [$F(1,224) = 2.61$, $p = 0.1074$] or interaction effects ($p > 0.1$ for all interactions).

Total dendritic length was also analyzed in the apical and basal dendritic trees of CA3 pyramidal neurons. In males, a significant interaction effect in the apical dendritic tree was observed between genotype and treatment ($F(1,16) = 10.15$, $p = 0.0057$), associated with an effect of finasteride treatment in the 3xTg but not the wild type males (Tukey-Kramer test: 3xm-V vs. 3xm-F, $p = 0.0183$) (Fig. 2 E). In females, significantly lower total apical dendritic length was observed in the 3xTg-AD animals (Unpaired two-tailed *t*-test; $t = 3.583$, $p = 0.0072$). No statistically significant effects of either genotype or sex were observed in the basal dendritic tree [Males: two-way ANOVA genotype; $F(1,16) = 0.0016$, $p = 0.9690$; treatment; $F(1,16) = 0.0061$, $p = 0.9388$. Females wild type vs 3xTg-AD: unpaired two-tailed *t*-test; $t = 0.8983$, $p = 0.3953$] (Fig. 2 F).

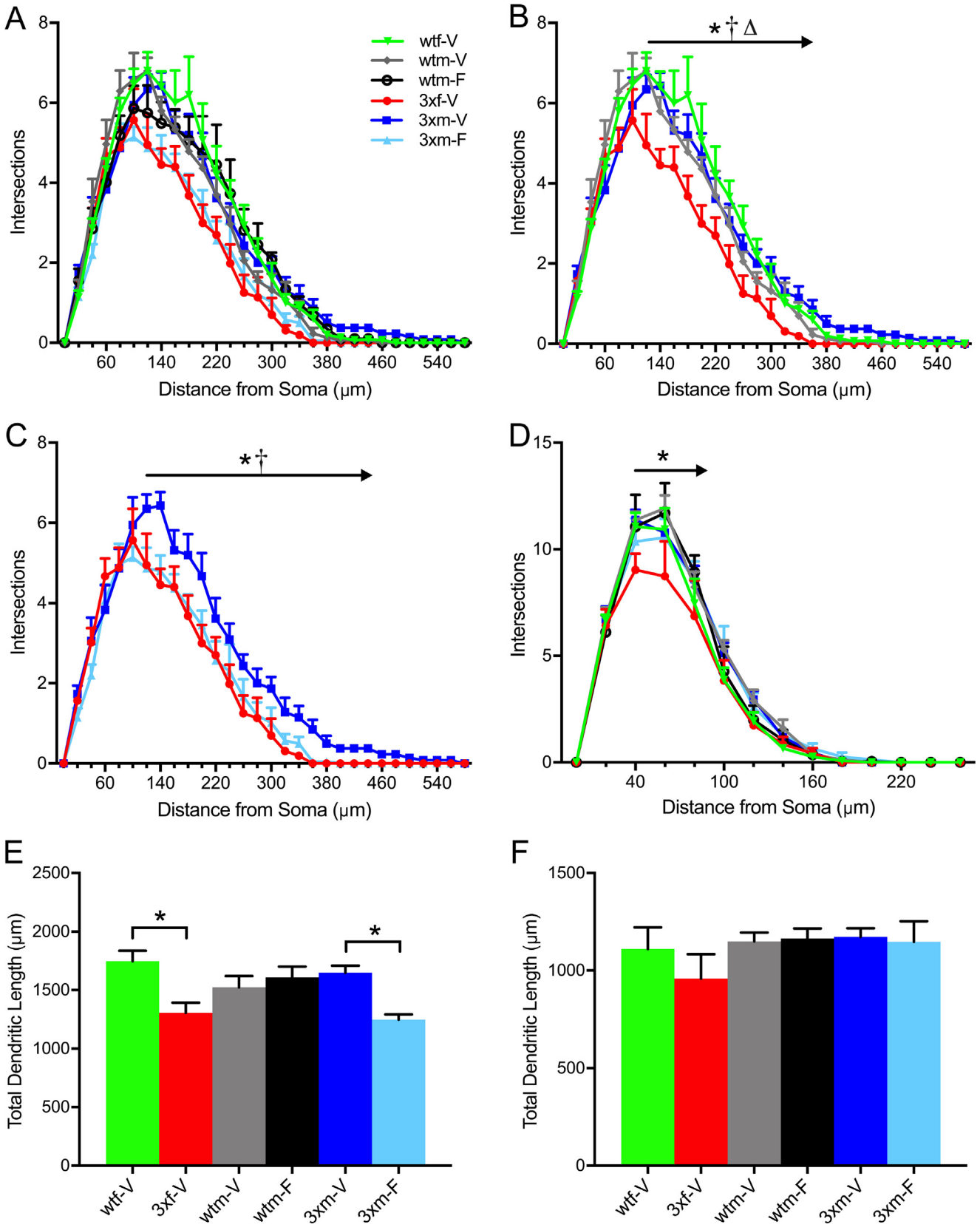
A
B
C
D
E
F
wtf-V
wtm-V
wtm-F
3xf-V
3xm-V
3xm-F
Intersections
Distance from Soma (μm)
Total Dendritic Length (μm)
*
†
Δ

Male 3xTg-AD mice exhibit reduced dendritic branching in CA1, compared to wild-type animals. In males, significant overall treatment [three-way ANOVA; $F(1,408) = 4.04$, $p = 0.045$], genotype [$F(1,408) = 44.61$, $p < 0.0001$] and distance from cell body-dependent [$F(23,408) = 125.9$, $p < 0.0001$] effects were observed, with a significant genotype × treatment interaction [$F(1,408) = 5.30$, p0.0219] (Fig. 3 A). Analysis of the data from vehicle treated males and females revealed significant genotype [$F(1,408) = 33.30$, $p < 0.0001$] and distance from cell body- [$F(23,408) = 99.33$, $p < 0.0001$] dependent differences, but no significant sex [$F(1,408) = 1.206$, $p = 0.2729$] difference, or sex × genotype [$F(1,408) = 3.558$, $p = 0.06$] interactions.

In the basal CA1 dendritic tree, the only differences observed in males were dependent on the distance from the cell body [$F(9,170) = 134.46$, $p < 0.0001$]. No significant overall treatment [$F(1,170) = 0.478$, $p = 0.490$] or genotype dependent [$F(1,170) = 0.808$, $p = 0.370$] effects were observed. Comparison of males and females in the vehicle treated animals also showed significant effects of distance from the cell body [$F(9,170) = 129.27$, $p < 0.0001$] but no sex [$F(1,224) = 15.12$, $p = 0.0001$] or genotype dependent [$F(1,224) = 2.61$, $p = 0.1074$] effects.

There was a significant reduction in total apical CA1 dendrite length in the 3xTg-AD males ($F(1,17) = 12.25$, $p = 0.0027$) but no overall treatment effect [$F(1,17) = 1.162$, $p = 0.2962$] (Fig. 3 E). Differences between the wild type and 3xTg-AD animals in females were not statistically significant [Unpaired two-tailed *t*-test; $t = 1.209$, $p = 0.2612$]. No significant treatment or genotype dependent effects were observed in the basal CA1 dendrites (Fig. 3 F).

Dendritic spines

Finasteride treatment in males differentially decreased spine density in the CA3 apical dendritic tree. Afferent inputs to the hippocampus terminate on dendritic spines in different parts of the apical dendritic trees of pyramidal neurons, depending on the origin of the projections. Therefore, dendritic spine density was determined separately for secondary dendrites of the apical dendritic tree in proximal, medial, and distal segments relative to the cell body in both the CA3 and CA1 hippocampal subfields, from all animals studied for hippocampal dendritic branching.

In CA3 (Fig. 4), no significant overall treatment or genotype-dependent effects were detected in the proximal segment. [Two-way ANOVA treatment; $F(1,16) = 7.887$, $p = 0.0126$; genotype $F(1,17) = 0.3504$, $p = 0.5617$]. In the medial segment, differences between wild type and 3xTg-AD mice did not reach the limit of statistical significance [$F(1,16) = 4.392$, $p = 0.0524$], but spine density was significantly higher in the vehicle treated males than after finasteride treatment [$F(1,16) = 16.83$, $p = 0.0008$]. In females, by contrast, spine density was significantly higher in the wild type than in 3xTg-AD mice (*t*-test; $t = 4.036$, $p = 0.0050$). In the distal CA3 dendrites, significant genotype-dependent differences were observed in both males [$F(1,16) = 16.67$, $p = 0.0009$] and females [*t*-test; $t = 4.993$, $p = 0.0016$]. However, in the males, the effects of finasteride were not statistically significant [$F(1,16) = 3.545$, $p = 0.0780$] (Fig. 4 D).

Dendritic spine density of CA1 pyramidal neurons was differentially reduced across the apical dendritic tree of 3xTg-AD mice. In CA1, as in CA3, no significant overall treatment or genotype-dependent effects were detected in the proximal segment of the apical dendrites [Two-way ANOVA treatment; $F(1,17) = 1.562$, $p = 0.2283$; genotype $F(1,17) = 0.894$, $p = 0.3576$]. However, in females spine density in the proximal segment was significantly higher in wild type than in 3xTg-AD animals [*t*-test; $t = 3.004$, $p = 0.0148$] (Fig. 5B). In the medial segment, significant differences were observed between male wild type and 3xTg-AD mice $F(1,17) = 18.08$, $p = 0.0005$, and between vehicle-treated and finasteride treated animals [$F(1,17) = 10.79$, $p = 0.0044$], but genotype dependent differences were not observed in females [*t*-test; $t = 0.8868$, $p = 0.3983$] (Fig. 5C). In the distal CA1 dendrites, significant genotype-dependent differences were observed in males [$F(1,16) = 16.67$, $p = 0.0009$] but not females [*t*-test; $t = 1.875$, $p = 0.0936$]. The effects of finasteride on distal spine

Fig. 2. Dendritic branching and length in the CA3 hippocampal subfield. **(A)** Dendritic branching of CA3 pyramidal neurons was examined using Sholl (1953) analysis, in all treatment groups. Panel A shows the means ± SEM of the number of intersections at different distances from the cell body in each of the six treatment groups. Each point represents the mean of data from independent observations in 5 animals. Panels B and C show subsets of the data, separated to allow differences between the treatment groups to be seen more clearly. Panel B shows data from wild type and 3xTg-AD females and males, without finasteride treatment: 3xTg-AD females had reduced dendritic branching compared to wild type males or females. Panel C compares 3xTg-AD males and females to 3xTg males treated with finasteride. Finasteride treatment of 3xTg-AD males reduced dendritic branching to levels indistinguishable from those in 3xTg-AD females **(C)**. Basal dendritic branching in CA3 was slightly but significantly reduced in 3xTg-AD females compared to males **(D)**. Total apical dendritic length was reduced in 3xTg-AD females compared to wild-type females, and finasteride reduced apical dendritic length in 3xTg-AD males **(E)**. No overall changes were observed in basal dendritic length **(F)**. All points or bars on graphs represent mean ± SEM ($n = 5$ each from an individual mouse, in in each treatment group). In panels B-D, * indicates $p < 0.05$ for 3xf-V vs. 3xm-V. In panel B, † and Δ indicate $p < 0.05$ for 3xf-V vs. wtf-V and wtm-V, respectively. In panel C, † and Δ indicate $p < 0.05$ for 3xm-V vs. 3xF-V and 3xm-F respectively (Tukey-Kramer multiple range test). In panels E and F, * indicates $p < 0.05$ for the comparisons indicated by brackets (non-paired t test).

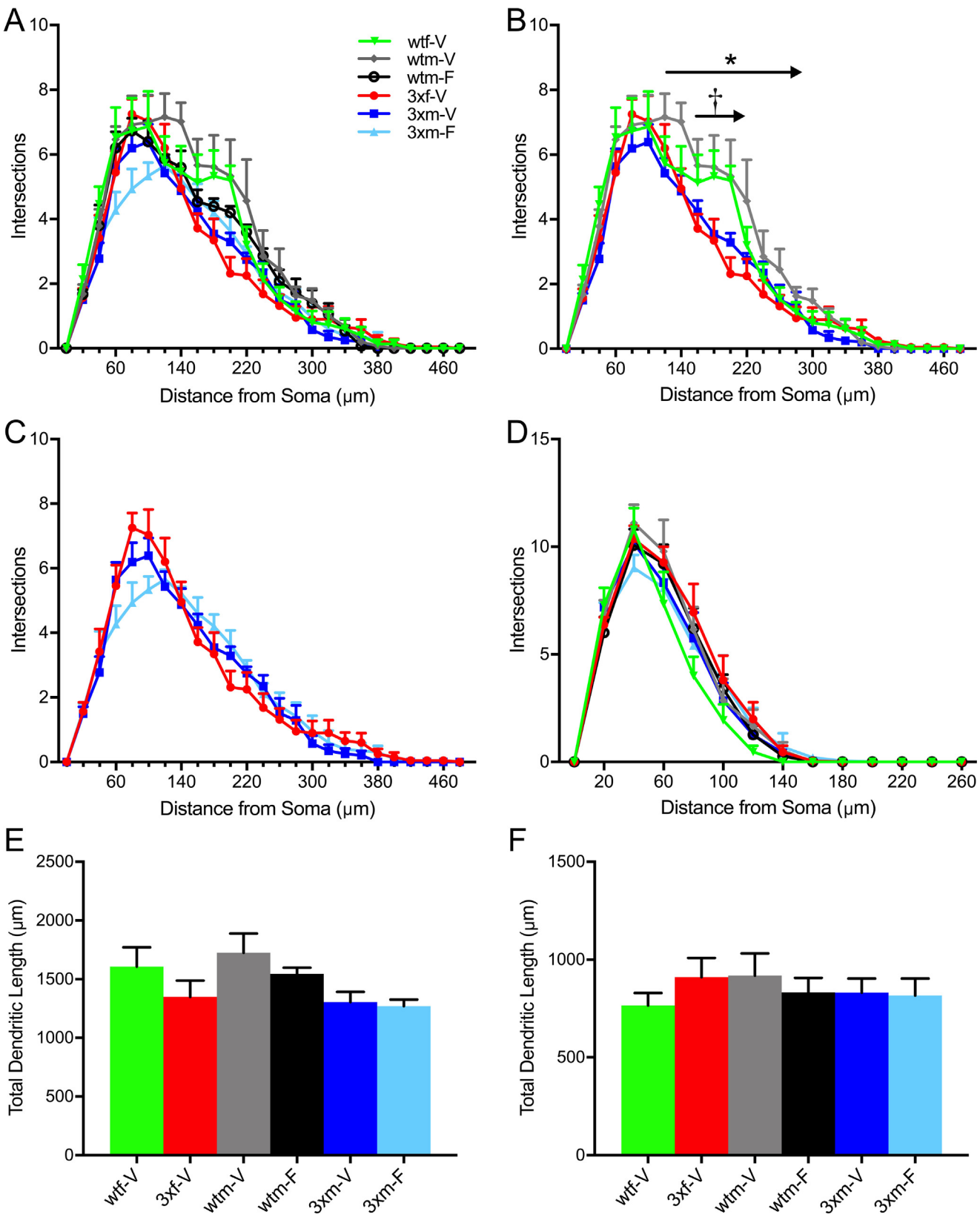

Fig. 3. Dendritic branching and length in the CA1 hippocampal subfield. Dendritic branching of CA1 pyramidal neurons is displayed for all treatment groups **(A)**. As with Fig. 1, subsets of the data are reproduced for clarity in panels B and C. **(B)** 3xTg-AD mice had reduced apical dendritic branching in CA1 compared to wild-types of either sex (* and † represent $p < 0.05$ for 3xf-V vs. wtf-V and 3xm-V vs. wtm-V, respectively; Tukey-Kramer multiple range test $p < 0.05$) **(C)**. Finasteride treatment of 3xTg-AD males did not further reduce branching. No significant differences in basal dendritic branching **(D)**, total apical dendritic length **(E)**, or total basal dendritic length **(F)** were observed between groups. All points or bars on graphs represent mean ± SEM (n = 5–6 mice/group).

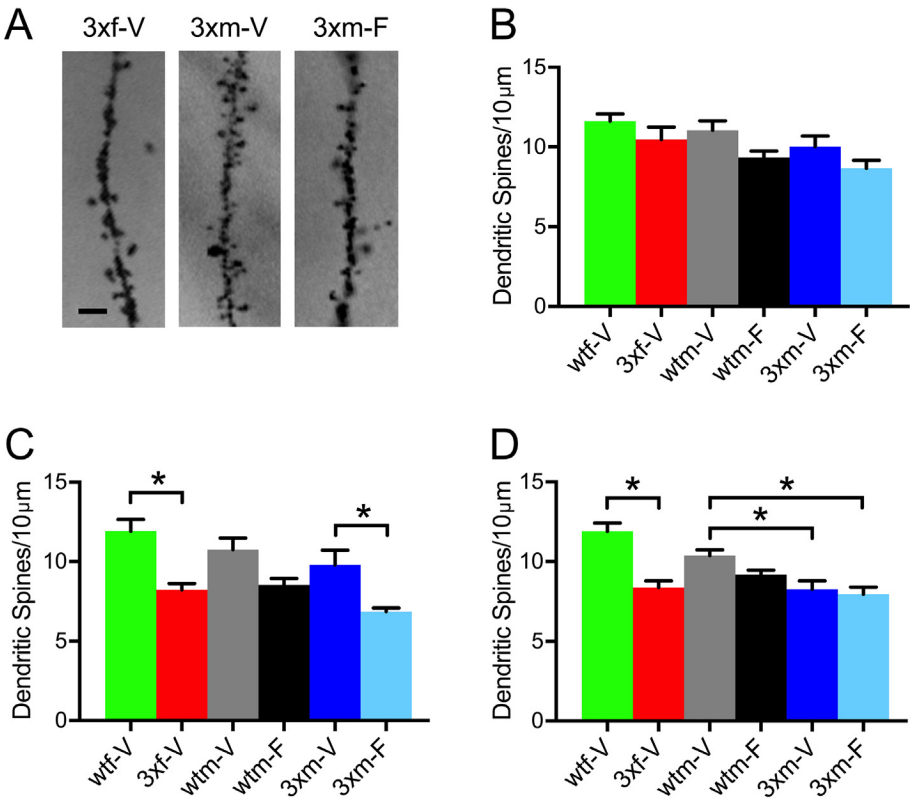

Fig. 4. Dendritic spine density in the CA3 hippocampal subfield. Representative micrographs from the medial segment of CA3 apical dendrites are shown in **(A)**. The horizontal black scale bar at the foot of the left-hand panel correspond to 10 μm. **(B)** No significant differences were observed in the proximal dendritic segment between treatment groups. **(C)** 3xTg-AD females had reduced dendritic spine density in the medial segment, compared to wild type controls (unpaired t test $p = 0.005$). This genotype difference was not seen in males; but finasteride treatment of 3xTg-AD males significantly reduced spine density * $p < 0.05$ Tukey-Kramer multiple range test. **(D)** In the distal dendritic segment, 3xTg-AD mice had reduced dendritic spine density, compared to wild-type animals of the same sex. Finasteride treatment of males had no significant effect. Bars on graphs represent the means ± SEM of average spine densities determined from 4-5 mice/group.

density in males were not statistically significant [$F(1,17) = 2.915$, $p = 0.1059$] (Fig. 5 D).

Proteins involved in signaling and pathology in AD

3xTg-AD females displayed significantly higher hippocampal Aβ levels than 3xTg-AD males. Levels of Aβ were evaluated in whole hippocampal lysate by western blot in the other halves of the brains studied for dendritic morphology, and in various hippocampal subfields by IHC in the remaining animals from each treatment group. In whole hippocampal lysates, Aβ was detectable by Western blot only in 3xTg-AD mice, of both sexes (Fig. 6A). Aβ levels in males were unaffected by finasteride treatment [two-way ANOVA; $F(1,17) = 0.0059$, $p = 0.9398$].

Regional Aβ immunoreactivity was evaluated by IHC at anterior, middle, and posterior levels of the hippocampus (equivalent to dorsal, rostral-ventral, and caudal-ventral hippocampus, respectively). In all subfields, stronger labeling was observed in female than in male 3xTg-AD mice. (Fig. 6B-H). Although there was considerable regional heterogeneity in staining in males, in all regions examined there was no significant effects of finasteride treatment on Aβ immunoreactivity ($p > 0.05$ for all comparisons).

Effects of finasteride on hippocampal ERK phosphorylation and site-specific phosphorylation of Tau in male 3xTg-AD mice. We have previously reported that 3α-diol protects neurons and neuronal cells in culture from neurotoxicity induced by Aβ and oxidative stressors, and this protection was associated with inhibition of ERK phosphorylation (Mendell et al., 2016, 2018). We therefore investigated whether any differences in hippocampal ERK phosphorylation resulted from inhibition of 5α reductase. Three way factorial ANOVA (genotype, ERK isoform and finasteride treatment) revealed a highly significant difference between wild type and 3xTg-AD males [$F(1,34) = 23.73$, $p < 0.0001$]. However, no significant effect of finasteride treatment was observed [$F(1,34) = 0.579$, $p = 0.4521$]. Comparing the sexes by ANOVA for the results in vehicle treated animals likewise revealed differences between the wild type and 3xTg-AD animals [3-way ANOVA $F(1,36) = 8.021$, $p = 0.0075$] but no sex-dependent difference in ERK phosphorylation [$F(1,36) = 2.229$, $p = 0.1442$] (Fig. 7A).

Hyperphosphorylation of Tau results in destabilization of this structural protein, eventually resulting in the formation of neurofibrillary tangles (Grundke-Iqbal et al., 1987; Del et al., 1996; Gotz, 2001). In 3xTg-AD mice, tangle pathology has been shown to occur around 12 months of age (Oddo et al., 2003), with hyperphosphorylation of Tau beginning earlier. We therefore evaluated levels of Tau phosphorylated at Serine 202 (P-Tau Ser202) and Serine 396 (P-Tau Ser396) – two sites that are associated with AD (Lee et al., 1991; Bramblett et al., 1993; Maccioni et al., 2006; De Felice et al., 2008) – as well as total Tau protein. Although P-Tau Ser202 levels tended to be higher in 3xTg-AD males than in the wild type controls, this difference was not statistically significant [$F(1,17) = 1.887$, $p = 0.1874$]. In females, however, P-Tau Ser202 levels were significantly higher in 3xTg-AD than in wild type animals [t-test; $t = 3.768$, $p = 0.0044$] (Fig. 7 B). For P-Tau Ser396, the pattern was reversed: for P-Tau Ser396 was significantly elevated in male 3xTg-AD mice, [$F(1,17) = 6.261$, $p = 0.0228$] but not in females [t-test; $t = 0.5636$, $p = 0.5868$] (Fig. 7 C). The effects of finasteride treatment were less pronounced

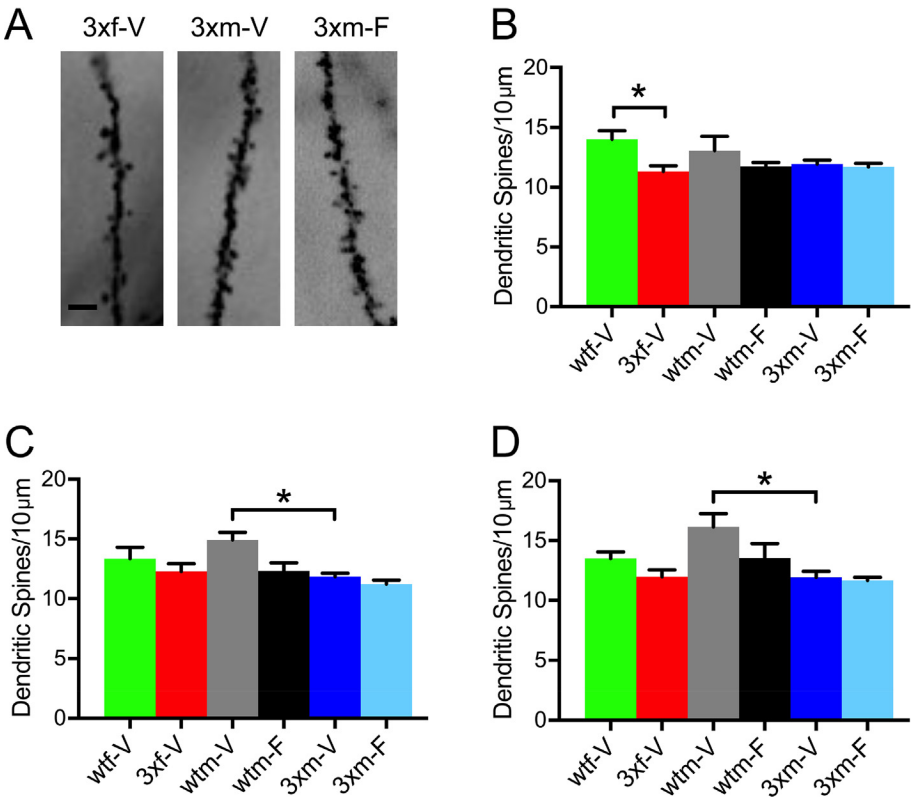

Fig. 5. Dendritic spine density in the CA1 hippocampal subfield. Representative micrographs from the medial segment of CA1 apical dendrites are shown in **(A)**. The horizontal black scale bar at the foot of the left-hand panel correspond to 10 μm. **(B)** 3xTg-AD females, but not males, had reduced dendritic spine density in the proximal segment of CA1 apical dendrites, compared to wild type controls. 3xTg-AD males, but not females, had reduced dendritic spine density in the medial **(C)** and distal **(D)** segments. Finasteride treatment of males did not have a significant effect. Bars on graphs represent mean ± SEM (n = 5–6 mice/group). * indicates significant differences for the comparisons indicated by brackets (t test p = 0.0016 for females; $p < 0.05$, Tukey-Kramer multiple range test, for males).

than those of either sex or the 3xTg-AD genotype. Although there was an overall trend towards increased Tau phosphorylation in the finasteride treated animals [3-way ANOVA performed on the results in males for both Tau phosphorylation sites: genotype $F(1,34) = 19.73$, $p < 0.0001$; Treatment effect: $F(1,34) = 5.354$, $p = 0.0269$; phosphorylation site: $F(1,34) = 0.034$, $p = 0.881$] this effect was not statistically significant when the results for P-Tau Ser202 or P-Tau Ser396 were analyzed separately [Two way ANOVA, finasteride treatment effect P-Tau Ser202 $F(1,17) = 2.788$, $p = 0.1133$; P-Tau Ser396 $F(1,17) = 2.82$, $p = 0.1114$]. Total Tau did not differ significantly between vehicle and 3xTg-AD mice, or between vehicle and finasteride treated animals (Fig. 7 D).

Hippocampal GFAP, NeuN and steroidogenic enzyme levels. Glial cell infiltration and neuronal cell death are prominent aspects of AD pathophysiology (Smale et al., 1995; Mattson, 2004), potentially altering the expression of glial fibrillary acidic protein (GFAP) and NeuN. The forward and backward interconversion reactions between DHT and 3α-diol are mediated by 3α-hydroxysteroid dehydrogenase type 3 (3α-HSD3) and 17β-hydroxysteroid dehydrogenase type 10 (17β-HSD10), respectively (Porcu et al., 2016). 17β-HSD10 has been reported to be elevated in the brains of patients with AD. It therefore seemed possible that the expression of these markers could have been altered in 3xTg mice, or by finasteride treatment. Western blot analysis, however, revealed no statistically significant differences between treatment groups in the levels of GFAP, NeuN, 3α-HSD3 or 17β-HSD10 (data not shown).

DISCUSSION

The results presented in this study are consistent with the hypothesis that 5α-reduced neurosteroids may play a role in protecting 3xTg-AD male mice against some aspects of the neuropathology observed in these animals. Several studies have demonstrated that exogenously administered testosterone and DHT can protect against various aspects of pathology and cognitive impairments in GDX 3xTg-AD animals (Rosario et al., 2006, 2010, 2012; George et al., 2013), and there is substantial evidence that AR-mediated neuroprotection contributes to sex differences in the development and severity of AD. However, to the best of our knowledge, this is the first study demonstrating that inhibition of 5α-reduction affects the maintenance of normal short-term memory and hippocampal structure in this model of AD.

Previous studies have demonstrated that the progesterone-derived neurosteroid allopregnanolone protects 3xTg-AD mice against various aspects of pathology, including reduction of Aβ accumulation, improvement of learning and memory, and stimulation of neurogenesis by inducing proliferation of neural precursor cells (Wang et al., 2010; Chen et al., 2011a, 2011b; Singh et al., 2012). Allopregnanolone and 3α-diol are synthesized from progesterone and testosterone, respectively, through identical sequential reduction steps by 5α-reductase and 3α-HSD. They share the 3α-hydroxy, 5α-reduced structure that is typical of inhibitory $GABA_AR$-modulating neurosteroids, though allopregnanolone is more potent in this regard (Reddy and Jian, 2010). However, both neurosteroids have also been reported to improve various aspects of cellular function through $GABA_AR$-independent mechanisms *in vitro* (Grimm et al., 2014; Mendell et al., 2016, 2018; Taleb et al., 2018), where 3α-diol appears to be effective at lower concentrations. Allopregnanolone and 3α-diol are both present in the brain of male 3xTg-AD mice at

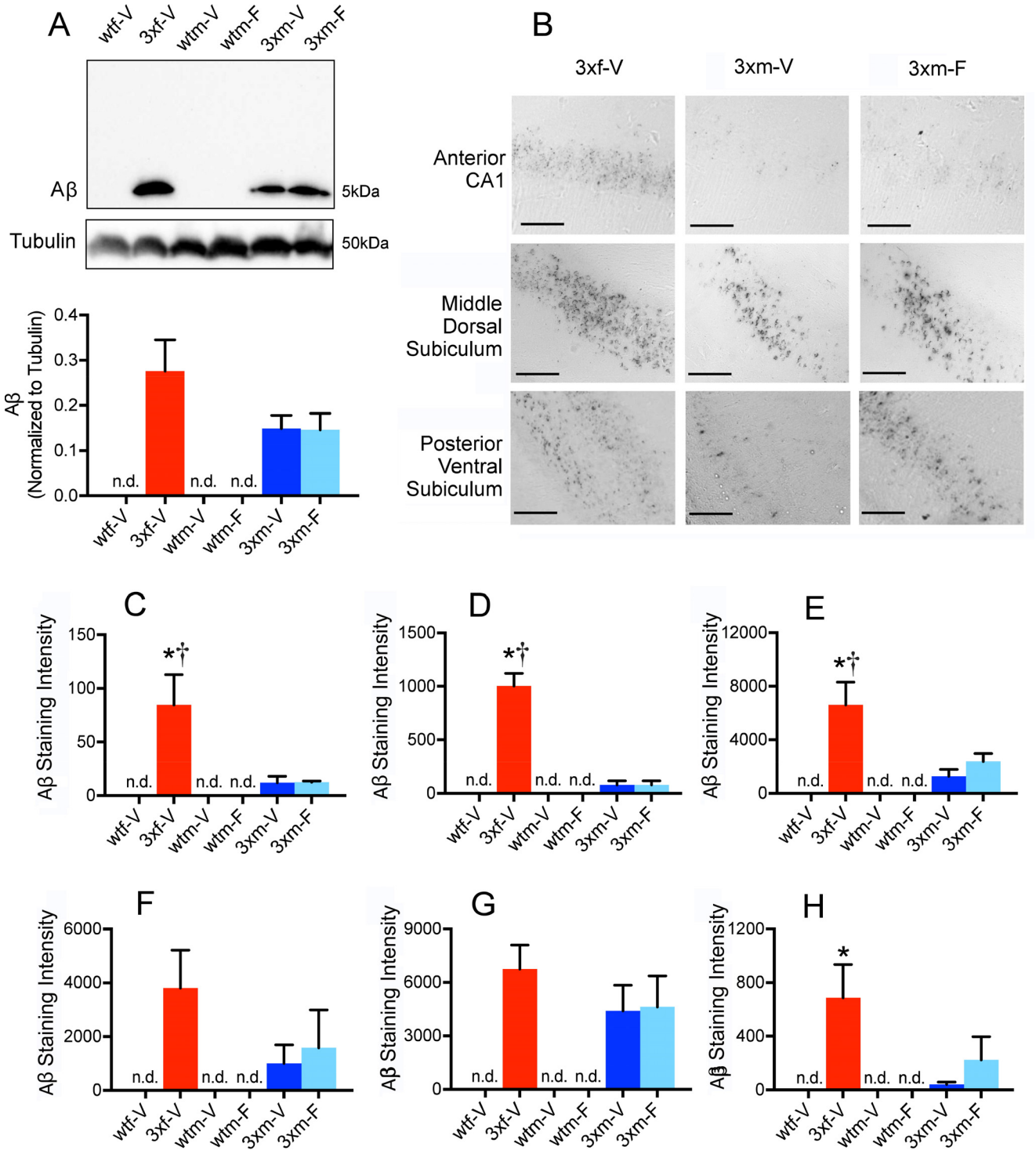

Fig. 6. Amyloid β levels in the hippocampus. **(A)** Representative western blots and densitometric analysis for amyloid β (Aβ) levels in whole hippocampal lysate, demonstrating elevated Aβ in 3xTg-AD mice. **(B)** Representative micrographs of sections from anterior CA1, middle dorsal subiculum, and posterior ventral subiculum from 3xTg-AD mice stained with an antibody against Aβ. Horizontal black scale bars on each panel correspond to 100 μm. 3xTg-AD mice had detectable staining in all areas of the hippocampus examined, while wild-type animals did not. Aβ immunostaining intensity, assessed as the number of immunostained pixels over background using NIH Image J software (Girish and Vijayalakshmi, 2004) was significantly higher in 3xTg-AD females compared to males treated with either vehicle or finasteride in the anterior CA1, middle CA1, and middle dorsal subiculum areas (C-E). No significant differences in Aβ staining were present between 3xTg-AD females and males in posterior CA1 or posterior dorsal subiculum (F-G). 3xTg-AD females had significantly elevated Aβ staining in posterior ventral subiculum compared to 3xTg-AD males treated with vehicle, but not those treated with finasteride **(H)**. All bars on graphs represent mean ± SEM of data from 4-6 mice/group). * and † represent $p < 0.05$ for 3xf-V vs. 3xm-V and 3xm-F, respectively.

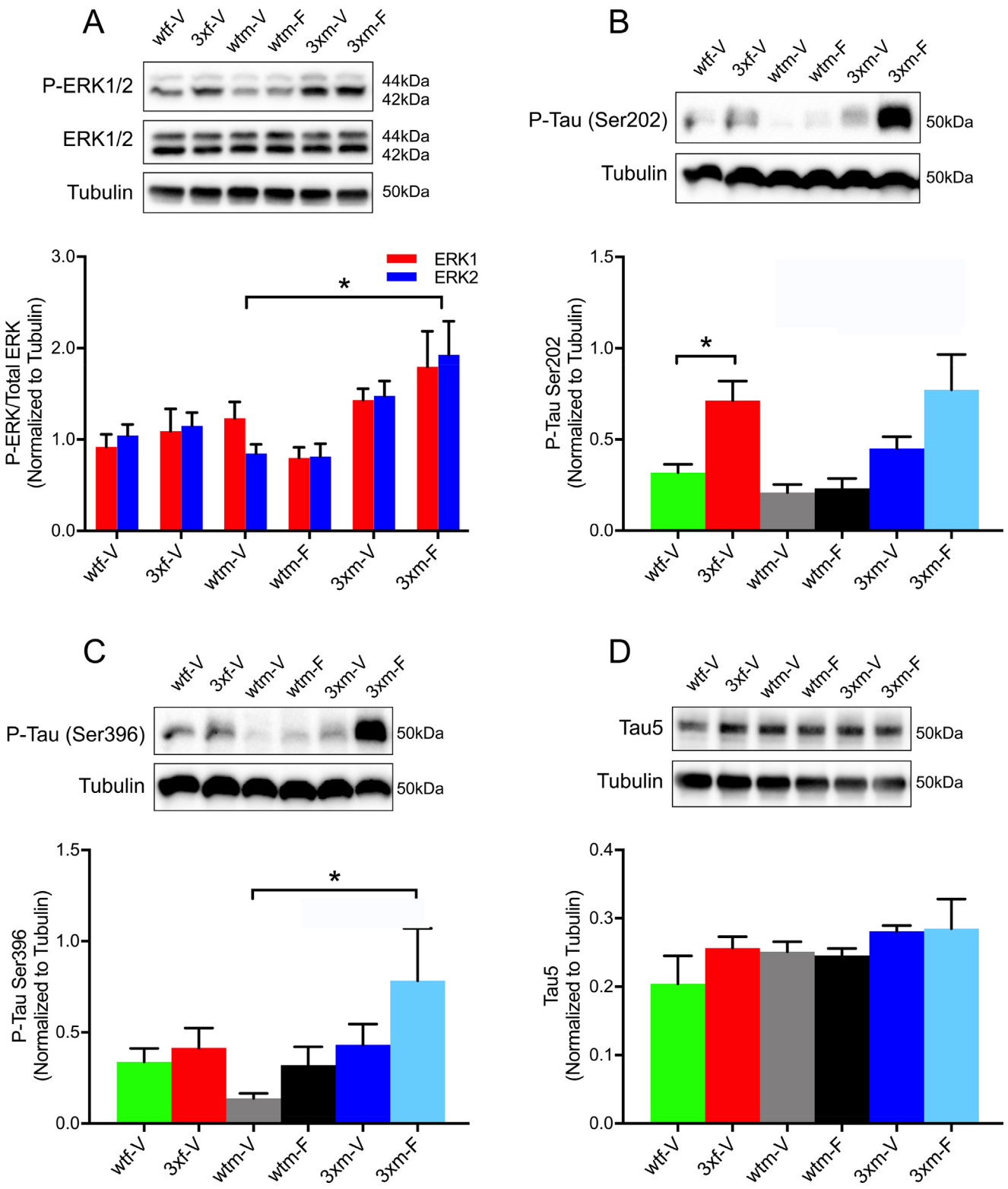

Fig. 7. ERK and tau phosphorylation in the hippocampus. **(A)** Representative western blots and densitometric analysis of whole hippocampal lysate for ERK, demonstrating elevated ERK phosphorylation in 3xTg-AD mice, compared to wild type animals. * 3-way ANOVA revealed significant effects of genotype [$F(1,34)$ 23.7, $p < 0.0001$] but not finasteride treatment [$F(1,34)$ 0.579, $p = 0.4521$] in males. Significant differences between wild type and 3xTg mice were not observed in females (t test $p > 0.05$). (B-D) Representative western blots and quantitative densitometric analysis for tau phosphorylated at Serine 202 **(B)** or Serine 396 **(C)** compared to total Tau **(D)**, demonstrating increased P-Tau in 3xTg-AD mice. Bars on graphs represent mean ± SEM ($n = 5$–6 mice/group). * represents $p < 0.05$ for the comparisons indicated by horizontal brackets. Although finasteride treatment increased mean Serine 202 and Serine 396 phosphorylated Tau levels, this effect was not statistically significant compared to the vehicle treated male controls by 2-way ANOVA, for either site-specific tau isoform ($p = 0.113$ and 0.0111, respectively).

concentrations that have been shown to be relatively unchanged during aging and advancing stages of pathology (Caruso et al., 2013). Allopregnanolone, but not 3α-diol, has been reported to decrease in the brains of both men and women with AD (Bernardi et al., 2000; Yang and He, 2001; Marx et al., 2006; Smith et al., 2006; Naylor et al., 2010). Both steroids may act to oppose the neurotoxic effects of AD-related pathology.

Sex differences in dysregulation of dendritic morphology in 6–7 month old 3xTg-AD mice were found to be hippocampal subfield-specific, with females having reduced dendritic branching in both the CA1 and CA3 subfields, while males only had reduced branching in CA1. The CA3 subfield is essential for early acquisition and encoding of contextual and spatial representations, as well as spatial pattern separation and completion related to short-term memories, but has minimal role in memory retrieval after a longer delay (Lee and Kesner, 2004; Kesner, 2013; Rolls, 2013; Cherubini and Miles, 2015). The CA1 subfield, however, plays a role in the rapid acquisition as well as the long-term retrieval of contextual memory, including spatial information, which relates to its role as the major output subfield within the hippocampal formation (McClelland and Goddard, 1996; Lee and Kesner, 2004). Interestingly, some studies have suggested that the CA3 subfield is relatively less affected in AD (Braak and Braak, 1991; Price et al., 1991; West et al., 1994; reviewed in Small et al., 2011), while other studies suggest that synaptic dysfunction, morphological dysregulation, pathophysiological markers, and apoptotic cells are present in both CA1 and CA3 in rodent models (Nava-Mesa et al., 2013) and humans (Smale et al., 1995; Yassa et al., 2010; reviewed in Llorens-Martin et al., 2014). The present findings suggest that subfield-specific effects on dendritic morphology are present in male 3xTg-AD mice, but that females have impairments in both subfields.

We observed elevated hippocampal Aβ levels in all 3xTg-AD mice, while wild-type mice did not have detectable levels of Aβ. Female 3xTg-AD mice had significantly greater immunoreactivity than males in several areas of the dorsal and ventral hippocampus, consistent with other reports in both the hippocampus and other areas of the brain in this mouse model (Hirata-Fukae et al., 2008; Carroll et al., 2010; Perez et al., 2011). Aβ immunoreactivity was more widely dispersed throughout the ventral hippocampus (middle and posterior levels of the brain in this study); the dorsal hippocampus (anterior level) had considerably lower immunoreactivity, which was primarily localized to the CA1 subfield. These findings are consistent with a study evaluating the spatial and temporal pattern of Aβ deposition in 3xTg-AD mice, which reported that pathology was more prominent at an earlier age in the caudal/posterior parts of the hippocampus (Mastrangelo and Bowers, 2008). Finasteride treatment in male 3xTg-AD mice did not appear to significantly alter Aβ. The subiculum is an important output structure of the hippocampal formation, receiving inputs from multiple levels of CA1 pyramidal neurons (O'Mara, 2005). As high Aβ levels were detected in the subiculum and CA1 subfield at all levels of the hippocampus, it is possible that a spatial progression of Aβ deposition throughout the hippocampus occurs, originating in the CA1 subfield. Interestingly, minimal Aβ immunoreactivity was detected in the CA3 subfield, even though this area displayed significant sex differences in dendritic morphology and a reduction in dendritic branching after finasteride treatment. The limited Aβ deposition at early-mid disease stages in CA3 is consistent with earlier reports of the progression of pathophysiology in AD (Braak and Braak, 1991; Price et al., 1991; West et al., 1994; reviewed in Small et al., 2011). Dysregulation of dendritic morphology of CA3 pyramidal neurons induced by finasteride may occur through mechanisms not directly related to Aβ deposition.

Dysregulated phosphorylation of intracellular signaling kinases have been shown to contribute to Tau hyperphosphorylation and neuronal death (Drewes et al., 1992; Pei et al., 2002; Chu et al., 2004; Harris et al., 2004; Young et al., 2006; Zhuang and Schnellmann, 2006; Feld et al., 2014; Arora et al., 2015; Li and Qian, 2016; Kirouac et al., 2017). In this study, an overall difference in ERK phosphorylation was observed between wild-type and 3xTg-AD mice, regardless of finasteride treatment (Fig. 7A). A previous study demonstrated that elevated ERK phosphorylation in the prefrontal cortex was correlated with ORM deficits in 6-month old 3xTg-AD mice, and that inhibition of ERK phosphorylation reversed the memory impairments (Feld et al., 2014). As finasteride-treated male 3xTg-AD mice were the only group with both elevated ERK phosphorylation and impaired short-term ORM in the present study, it is possible that these two findings are related. There are two important caveats to this interpretation of the data, however. First, we only examined ERK phosphorylation in the hippocampus. It is possible that ERK phosphorylation may be differentially affected by inhibition of 5α reductase, in other regions of the brain that contribute to cognitive behavior. Second, although phospho-ERK levels were elevated in the 3xTg-AD males, compared to wild type animals, finasteride treatment did not significantly affect ERK phosphorylation (Fig. 7A). Additional experiments will be required to establish the relationship between ERK phosphorylation in different areas of the brain and memory impairment in 3xTg-AD mice, at different time points after finasteride treatment.

We also detected slight overall increases in Tau phosphorylation in 3xTg-AD mice (Fig. 7B, C). No changes in total Tau were observed. Hyperphosphorylation of the Ser202 and Ser396 residues has been widely associated with Tau pathology in AD (Lee et al., 1991; Bramblett et al., 1993; Maccioni et al., 2006; De Felice et al., 2008), and has previously been reported in 3xTg-AD mice (Oddo et al., 2003; Caccamo et al., 2007; Carroll et al., 2007). Ser202 has been shown to be a direct phosphorylation target of activated ERK (Harris et al., 2004; Lambourne et al., 2005; Qi et al., 2016). Up-regulation of ERK1/2 has been associated with the progression of neurofibrillary degeneration in AD brains (Pei et al., 2002), suggesting that elevated ERK phosphorylation may contribute to the increase in Tau phosphorylation observed in 3xTg-AD males. However, as noted in Results, a significant effect of finasteride treatment was

observed only when the Ser202 and Ser396 phosphorylation data were considered together, not when the Ser202 data were analyzed separately. Several other intracellular signaling proteins have also been proposed as modulators of Tau phosphorylation (Grimes and Jope, 2001; Jope and Johnson, 2004; Li and Qian, 2016; Kirouac et al., 2017), so the extent to which the observed increase in Tau phosphorylation is due to ERK activation remains to be established.

That ERK phosphorylation is not directly corelated with the behavioral outcome of finasteride treatment can also be seen in the data for wild-type males. Wild-type male mice treated with finasteride had phospho-ERK levels in their hippocampus that were not significantly different from vehicle-injected controls (Fig. 7A). However, they exhibited impaired long-term ORM (Fig. 1) and reduced hippocampal dendritic spine density (Figs. 4 and 5). Recent studies in men that have taken finasteride as a treatment for androgenic alopecia have reported cognitive and psychological symptoms following the termination of finasteride use, including memory impairments, depression, and anxiety (Ganzer et al., 2015; Melcangi et al., 2017). It is tempting to speculate that reduced hippocampal dendritic spine density may contribute to the development of cognitive and psychological symptoms (reviewed in Qiao et al., 2016) observed in patients with post-finasteride syndrome.

In summary, these data are consistent with the hypothesis that at least some of the neuroprotective effects conferred by testosterone in 3xTg-AD mice may be associated with the formation of 5α-reduced metabolites. What these metabolites are remains to be determined, since testosterone is not the only substrate for 5α-reductase in the brain. Inhibition of 5α-reductase in males would be expected to reduce tissue concentrations of a number of different bioactive steroids, including DHT and 3α-diol, as well as allopregnanolone (Caruso et al., 2013) and 5α-reduced metabolites of corticosterone, which is also (Sarkar et al 2011). Thus, the effects of finasteride treatment could potentially include contributions from reductions in the biosynthesis of multiple different 5α-reduced neurosteroids. It is also only a presumption that the effects are due to alterations in 5α-reductase activity in the brain. Since finasteride treatment reduces 5α-reduced steroid levels throughout the body (Finn et al 2006), it is conceivable that the effects could be secondary to change in peripheral steroid metabolism.

Regardless of the identity of the metabolites responsible, these data add further weight to the hypothesis that 5α-reductase may play an important role in regulating the neuroprotective effects of circulating steroids on the brain. Previous work has suggested that the administration of allopregnanolone (Wang et al., 2010; Chen et al., 2011a, 2011b; Singh et al., 2012) or synthetic analogs of this neurosteroid (Karout et al., 2016; Taleb et al., 2018) may enhance neuroprotection and neurogenesis in AD. The present results, together with previous *in vitro* observations on the effects of 3α-diol (Mendell et al., 2016,2018) suggest that 5α-reduced metabolites of testosterone could also potentially represent therapeutic alternatives for treatment of this disease.

CONFLICT OF INTEREST

The authors declare no competing financial interests.

ACKNOWLEDGEMENTS

This work was supported by Natural Sciences and Engineering Research Council of Canada (NSERC) Discovery Grants RGPIN-2015-04537 (NJM) and RGPIN-2018-400176 (BDW). ALM and SDC were the recipients of NSERC CGS-D scholarships and HW was the recipient of an NSERC CGS-M scholarship.

REFERENCES

Adams MM, Fink SE, Shah RA, Janssen WGM, Hayashi S, Milner TA, McEwen BS, Morrison JH (2002) Estrogen and aging affect the subcellular distribution of estrogen receptor-alpha in the hippocampus of female rats. J Neurosci 22:3608–3614.

Alzheimer's Association (2014) Alzheimer's Association Report: 2014 Alzheimers disease facts and figures. Alzheimer's Dement 10: e47–e92.

Arora K, Cheng J, Nichols RA (2015) Nicotinic acetylcholine receptors sensitize a MAPK-linked toxicity pathway on prolonged exposure to β-amyloid. J Biol Chem 290:21409–21420.

Bernardi F, Lanzone A, Cento RM, Spada RS, Pezzani I, Genazzani AD, Luisi S, Luisi M, Petraglia F, Genazzani AR (2000) Allopregnanolone and dehydroepiandrosterone response to corticotropin-releasing factor in patients suffering from Alzheimer's disease and vascular dementia. Eur J Endocrinol 142:466–471.

Braak H, Braak E (1991) Neuropathological stageing of Alzheimer-related changes. Acta Neuropathol 82:239–259.

Bradford MM (1976) A rapid and sensitive method for the quantitation of microgram quantities of protein utilizing the principle of protein-dye binding. Anal Biochem 72:248–254.

Bramblett GT, Goedert M, Jakes R, Merrick SE, Trojanowski JQ, Lee VMY (1993) Abnormal tau phosphorylation at Ser396in alzheimer's disease recapitulates development and contributes to reduced microtubule binding. Neuron 10:1089–1099.

Burry RW (2011) Controls for Immunocytochemistry: An Update. J Histochem Cytochem 59(1):6–12.

Caccamo A, Oddo S, Tran LX, LaFerla FM (2007) Lithium reduces tau phosphorylation but not Aβ or working memory deficits in a transgenic model with both plaques and tangles. Am J Pathol 170:1669–1675.

Carroll JC, Rosario ER, Chang L, Stanczyk FZ, Oddo S, LaFerla FM, Pike CJ (2007) Progesterone and Estrogen Regulate Alzheimer-Like Neuropathology in Female 3xTg-AD Mice. J Neurosci 27:13357–13365.

Carroll JC, Rosario ER, Kreimer S, Villamagna A, Gentzschein E, Stanczyk FZ, Pike CJ (2010) Sex differences in β-amyloid accumulation in 3xTg-AD mice: Role of neonatal sex steroid hormone exposure. Brain Res 1366:233–245.

Caruso D, Barron AM, Brown MA, Abbiati F, Carrero P, Pike CJ, Garcia-Segura LM, Melcangi RC (2013) Age-related changes in neuroactive steroid levels in 3xTg-AD mice. Neurobiol Aging 34:1080–1089.

Chen X, Nelson CD, Li X, Winters Ca, Azzam R, Sousa Aa, Leapman RD, Gainer H, Sheng M, Reese T (2011b) PSD-95 is required to sustain the molecular organization of the postsynaptic density. J Neurosci 31:6329–6338.

Chen S, Wang JM, Irwin RW, Yao J, Liu L, Brinton RD (2011a) Allopregnanolone promotes regeneration and reduces β-amyloid burden in a preclinical model of Alzheimer's disease. PLoS ONE:6.

Cherubini E, Miles R (2015) The CA3 region of the hippocampus: how is it? What is it for? How does it do it? Front Cell Neurosci 9:9–11.

Chu CT, Levinthal DJ, Kulich SM, Chalovich EM, DeFranco DB (2004) Oxidative neuronal injury: The dark side of ERK1/2. Eur J Biochem 271:2060–2066.
De Felice FG, Wu D, Lambert MP, Fernandez SJ, Velasco PT, Lacor PN, Bigio EH, Jerecic J, Acton PJ, Shughrue PJ, Chen-Dodson E, Kinney GG, Klein WL (2008) Alzheimer's disease-type neuronal tau hyperphosphorylation induced by Aβ oligomers. Neurobiol Aging 29:1334–1347.
Del C, Alonso A, Grundke-Iqbal I, Iqbal K (1996) Alzheimer's disease hyperphosphorylated tau sequesters normal tau into tangles of filaments and disassembles microtubules. Nat Med 2:783–787.
Drewes G, Lichtenberg-Kraag B, Döring F, Mandelkow EM, Biernat J, Goris J, Dorée M, Mandelkow E (1992) Mitogen activated protein (MAP) kinase transforms tau protein into an Alzheimer-like state. EMBO J 11:2131–2138.
Duarte-Guterman P, Lieblich SE, Chow C, Galea LAM (2015) Estradiol and GPER activation differentially affect cell proliferation but not GPER expression in the hippocampus of adult female rats. PLoS ONE 10:1–18.
Edinger KL, Frye CA (2004) Testosterone's analgesic, anxiolytic, and cognitive-enhancing effects may be due in part to actions of its 5α-reduced metabolites in the hippocampus. Behav Neurosci 118:1352–1364.
Ennaceur D, Delacour J (1988) A new one-trial test for neurobiological studies of memory in rats. 1: Behavioral data. Behav Brain Res 31:47–59.
Feld M, Krawczyk MC, Fustiñana MS, Blake MG, Baratti CM, Romano A, Boccia MM (2014) Decrease of ERK/MAPK overactivation in prefrontal cortex reverses early memory deficit in a mouse model of alzheimer's disease. J Alzheimer's Dis 40:69–82.
Finn DA, Beadles-Bohling AS, Beckley EH, Ford MM, Gililland KR, Gorin-Meyer RE, Wiren KM (2006) A New Look at the 5alpha-Reductase Inhibitor Finasteride. CNS Drug Rev 12:53–76.
Frye CA, Edinger KL, Lephart ED, Walf AA (2010) 3A-Androstanediol, But Not Testosterone, Attenuates Age-Related Decrements in Cognitive, Anxiety, and Depressive Behavior of Male Rats. Front Aging Neurosci 2:1–21.
Ganzer CA, Jacobs AR, Iqbal F (2015) Persistent Sexual, Emotional, and Cognitive Impairment Post-Finasteride: A Survey of Men Reporting Symptoms. Am J Mens Health 9:222–228.
George S, Petit GH, Gouras GK, Brundin P, Olsson R (2013) Nonsteroidal selective androgen receptor modulators and selective estrogen receptor β agonists moderate cognitive deficits and amyloid-β levels in a mouse model of Alzheimer's disease. ACS Chem Neurosci 4:1537–1548.
Girish V, Vijayalakshmi A (2004) Affordable image analysis using NIH Image/ImageJ. Indian J Cancer 41:47.
Gotz J (2001) Formation of Neurofibrillary Tangles in P301L Tau Transgenic Mice Induced by Abeta 42 Fibrils. Science (80-) 293:1491–1495.
Grimes CA, Jope RS (2001) The multifaceted roles of glycogen synthase kinase 3β in cellular signaling. Prog Neurobiol 65:391–426.
Grimm A, Schmitt K, Lang UE, Mensah-Nyagan AG, Eckert A (2014) Improvement of neuronal bioenergetics by neurosteroids: Implications for age-related neurodegenerative disorders. Biochim Biophys Acta – Mol Basis Dis 1842:2427–2438.
Grimm A, Biliouris EE, Lang UE, Götz J, Mensah-Nyagan AG, Eckert A (2016) Sex hormone-related neurosteroids differentially rescue bioenergetic deficits induced by amyloid-β or hyperphosphorylated tau protein. Cell Mol Life Sci 73:201–215.
Grundke-Iqbal I, Iqbal K, Tung Y-C, Quinlan M, Wisniewski H, Binder L (1987) Abnormal phosphorylation of the microtubule-associated protein? (tau) in Alzheimer cytoskeletal pathology. Alzheimer Dis Assoc Disord 1:202.
Hanamsagar R, Bilbo S (2016) Sex differences in neurodevelopmental and neurodegenerative disorders: Focus on microglial function and neuroinflammation during development. J Steroid Biochem Mol Biol 160:127–133.
Handa RJ, Pak TR, Kudwa AE, Lund TD, Hinds L (2008) An alternate pathway for androgen regulation of brain function: Activation of estrogen receptor beta by the metabolite of dihydrotestosterone, 5α-androstane-3β,17β-diol. Horm Behav 53:741–752.
Harris FM, Brecht WJ, Xu Q, Mahley RW, Huang Y (2004) Increased tau phosphorylation in apolipoprotein E4 transgenic mice is associated with activation of extracellular signal-regulated kinase. Modulation by zinc. J Biol Chem 279:44795–44801.
Hebert LE, Weuve J, Scherr PA, Evans DA (2013) Alzheimer disease in the United States (2010–2050) estimated using the 2010 census. Neurology 80:1778–1783.
Hirata-Fukae C et al (2008) Females exhibit more extensive amyloid, but not tau, pathology in an Alzheimer transgenic model. Brain Res 1216:92–103.
Hogervorst E, Williams J, Budge M, Barnetson L, Combrinck M, Smith A (2001) Serum total testosterone is lower in men with Alzheimer's disease. Neuro Endocrinol Lett 22:163–168.
Hogervorst E, Combrinck M, Smith A (2003) Testosterone and gonadotropin levels in men with dementia. Neuro Endocrinol Lett 24:203–208.
Hogervorst E, Bandelow S, Combrinck M, Smith AD (2004) Low free testosterone is an independent risk factor for Alzheimer's disease. Exp Gerontol 39:1633–1639.
Hsu B, Cumming RG, Waite LM, Blyth FM, Naganathan V, Le Couteur DG, Seibel MJ, Handelsman DJ (2015) Longitudinal relationships between reproductive hormones and cognitive decline in older men: The concord health and ageing in men project. J Clin Endocrinol Metab 100:2223–2230.
Jayaraman A, Carroll JC, Morgan TE, Lin S, Zhao L, Arimoto JM, Murphy MP, Beckett TL, Finch CE, Brinton RD, Pike CJ (2012) 17β-Estradiol and progesterone regulate expression of β-amyloid clearance factors in primary neuron cultures and female rat brain. Endocrinology 153:5467–5479.
Jope RS, Johnson GVW (2004) The glamour and gloom of glycogen synthase kinase-3. Trends Biochem Sci 29:95–102.
Karout M, Miesch M, Geoffroy P, Kraft S, Hofmann HD, Mensah-Nyagan AG, Kirsch M (2016) Novel analogs of allopregnanolone show improved efficiency and specificity in neuroprotection and stimulation of proliferation. J Neurochem 139:782–794.
Kesner R (2013) A process analysis of the CA3 subregion of the hippocampus. Front Cell Neurosci 7:78.
Kirouac L, Rajic AJ, Cribbs DH, Padmanabhan J (2017) Activation of Ras-ERK Signaling and GSK-3 by Amyloid Precursor Protein and Amyloid Beta Facilitates Neurodegeneration in Alzheimer's Disease. eNeuro 4. ENEURO.0149-16.2017.
Kritzer MF (2006) Regional, laminar and cellular distribution of immunoreactivity for ERβ in the cerebral cortex of hormonally intact, postnatally developing male and female rats. Cereb Cortex 16:1181–1192.
Lambourne SL, Sellers LA, Bush TG, Choudhury SK, Emson PC, Suh Y, Wilkinson LS (2005) Increased tau Phosphorylation on Mitogen-Activated Protein Kinase Consensus Sites and Cognitive Decline in Transgenic Models for Alzheimer ' s Disease and FTDP-17: Evidence for Distinct Molecular Processes Underlying tau Abnormalities. Mol Cell Biol 25:278–293.
Lee VM, Balin BJ, Otvos Jr L, Trojanowski JQ (1991) A68: a major subunit of paired helical filaments and derivatized forms of normal Tau. Science 251:675–678.
Lee I, Kesner RP (2004) Differential contributions of dorsal hippocampal subregions to memory acquisition and retrieval in contextual fear-conditioning. Hippocampus 14:301–310.
Levin-Allerhand JA, Lominska CE, Wang J, Smith JD (2002) 17α-estradiol and 17β-estradiol treatments are effective in lowering cerebral amyloid-β levels in AβPPSWE transgenic mice. J Alzheimer's Dis 4:449–457.
Li M, Qian S (2016) Gastrodin Protects Neural Progenitor Cells Against Amyloid Beta (1–42)-Induced Neurotoxicity and Improves Hippocampal Neurogenesis in Amyloid Beta (1–42)-Injected Mice. J Mol Neurosci 60:21–32.
Llorens-Martin M, Blazquez-Llorca L, Benavides-Piccione R, Rabano A, Hernandez F, Avila J, DeFelipe J (2014) Selective alterations of neurons and circuits related to early memory loss in Alzheimer's disease. Front Neuroanat 8:1–12.

Louth EL, Sutton CD, Mendell AL, MacLusky NJ, Bailey CDC (2017) Imaging neurons within thick brain sections using the Golgi-cox method. J Vis Exp:1–10.
Maccioni RB, Lavados M, Guillón M, Mujica C, Bosch R, Farías G, Fuentes P (2006) Anomalously phosphorylated tau and Aβ fragments in the CSF correlates with cognitive impairment in MCI subjects. Neurobiol Aging 27:237–244.
MacLusky NJ, Hajszan T, Prange-Kiel J, Leranth C (2006) Androgen modulation of hippocampal synaptic plasticity. Neuroscience 138:957–965.
Marx CE, Trost WT, Shampine LJ, Stevens RD, Hulette CM, Steffens DC, Ervin JF, Butterfield MI, Blazer DG, Massing MW, Lieberman JA (2006) The Neurosteroid Allopregnanolone Is Reduced in Prefrontal Cortex in Alzheimer's Disease. Biol Psychiatry 60:1287–1294.
Mastrangelo MA, Bowers WJ (2008) Detailed immunohistochemical characterization of temporal and spatial progression of Alzheimer's disease-related pathologies in male triple-transgenic mice. BMC Neurosci 9:1–31.
Mattson MP (2004) Pathways towards and away from Alzheimer's disease. Nature 430:631–639.
McClelland J, Goddard N (1996) Considerations arising from a complementary learning systems perspective on hippocampus and neocortex. Hippocampus 6:654–665.
Melcangi RC, Santi D, Spezzano R, Grimoldi M, Tabacchi T, Fusco ML, Diviccaro S, Giatti S, Carrà G, Caruso D, Simoni M, Cavaletti G (2017) Neuroactive steroid levels and psychiatric and andrological features in post-finasteride patients. J Steroid Biochem Mol Biol 171:229–235.
Mendell AL, Atwi S, Bailey CDC, McCloskey D, Scharfman HE, MacLusky NJ (2017) Expansion of mossy fibers and CA3 apical dendritic length accompanies the fall in dendritic spine density after gonadectomy in male, but not female, rats. Brain Struct Funct 222:587–601.
Mendell AL, Chung BYT, Creighton CE, Kalisch BE, Bailey CDC, MacLusky NJ (2018) Neurosteroid metabolites of testosterone and progesterone differentially inhibit ERK phosphorylation induced by amyloid β in SH-SY5Y cells and primary cortical neurons. Brain Res 1686:83–93.
Mendell AL, Creighton CE, Kalisch BE, MacLusky NJ (2016) 5α-Androstane-3α,17β-Diol Inhibits Neurotoxicity in SH-SY5Y Human Neuroblastoma Cells and Mouse Primary Cortical Neurons. Endocrinology 157:4570–4578.
Milner TA, McEwen BS, Hayashi S, Li CJ, Reagan LP, Alves SE (2001) Ultrastructural evidence that hippocampal alpha estrogen receptors are located at extranuclear sites. J Comp Neurol 429:355–371.
Milner TA, Ayoola K, Drake CT, Herrick SP, Tabori NE, McEwen BS, Warrier S, Alves SE (2005) Ultrastructural localization of estrogen receptor β immunoreactivity in the rat hippocampal formation. J Comp Neurol 491:81–95.
Mogi K, Takanashi H, Nagasawa M, Kikusui T (2015) Sex differences in spatiotemporal expression of AR, ERα, and ERβ mRNA in the perinatal mouse brain. Neurosci Lett 584:88–92.
Nava-Mesa MO, Jiménez-Díaz L, Yajeya J, Navarro-Lopez JD (2013) Amyloid-β induces synaptic dysfunction through G protein-gated inwardly rectifying potassium channels in the fimbria-CA3 hippocampal synapse. Front Cell Neurosci 7:1–14.
Naylor JC, Kilts JD, Hulette CM, Steffens DC, Blazer G, Ervin JF, Strauss JL, Allen TB, Massing MW, Payne VM, Youssef NA, Shampine LJ, Christine E (2010) Allopregnanolone Levels are Reduced in Temporal Cortex in Patients with Alzheimer's Disease Compared to Cognitively Intact Control Subjects. Biochim Biophys Acta 1801:951–959.
O'Mara S (2005) The subiculum: What it does, what it might do, and what neuroanatomy has yet to tell us. J Anat 207:271–282.
Oddo S, Caccamo A, Kitazawa M, Tseng BP, LaFerla FM (2003) Amyloid deposition precedes tangle formation in a triple transgenic model of Alzheimer's disease. Neurobiol Aging 24:1063–1070.
Pei JJ, Braak H, An WL, Winblad B, Cowburn RF, Iqbal K, Grundke-Iqbal I (2002) Up-regulation of mitogen-activated protein kinases ERK1/2 and MEK1/2 is associated with the progression of neurofibrillary degeneration in Alzheimer's disease. Mol Brain Res 109:45–55.
Perez SE, He B, Muhammad N, Oh KJ, Fahnestock M, Ikonomovic MD, Mufson EJ (2011) Cholinotrophic basal forebrain system alterations in 3xTg-AD transgenic mice. Neurobiol Dis 41:338–352.
Petanceska SS, Nagy V, Frail D, Gandy S (2000) Ovariectomy and 17beta-estradiol modulate the levels of Alzheimer's amyloid beta peptides in brain. Exp Gerontol 35:1317–1325.
Plassman B, Langa K, McCammon R, Fisher G, Potter G, Burke J, Steffens D, Foster N, Giordani B, Unverzagt F, Welsh-Bohmer K, Heeringa S, Weir D, Wallace R (2011) Incidence of dementia and cognitive impairment, not dementia in the United States. Ann Neurol 70:418–426.
Porcu P, Barron AM, Frye CA, Walf AA, Yang S, He X, Morrow AL, Panzica GC, Melcangi RC (2016) Neurosteroidogenesis today: Novel targets for neuroactive steroid synthesis and action and their relevance for translational research.
Price JL, Davis PB, Morris JC, White DL (1991) The distribution of tangles, plaques and related immunohistochemical markers in healthy aging and Alzheimer's disease. Neurobiol Aging 12:295–312.
Qi H, Prabakaran S, Cantrelle F-X, Chambraud B, Gunawardena J, Lippens G, Landrieu I (2016) Characterization of Neuronal Tau Protein as a Target of Extracellular Signal-regulated Kinase. J Biol Chem 291:7742–7753.
Qiao H, Li MX, Xu C, Bin Chen H, An SC, Ma XM (2016) Dendritic Spines in Depression: What We Learned from Animal Models. Neural Plast 2016:20–24.
Ramsden M, Nyborg AC, Murphy MP, Chang L, Stanczyk FZ, Golde TE, Pike CJ (2003) Androgens modulate β-amyloid levels in male rat brain. J Neurochem 87:1052–1055.
Reddy DS, Jian K (2010) The Testosterone-Derived Neurosteroid Androstanediol Is a Positive Allosteric Modulator of GABA A Receptors. J Pharmacol Exp Ther 334:1031–1041.
Rolls E (2013) A quantitative theory of the functions of the hippocampal CA3 network in memory. Front Cell Neurosci 7:98.
Rosario ER, Carroll JC, Oddo S, LaFerla FM, Pike CJ (2006) Androgens Regulate the Development of Neuropathology in a Triple Transgenic Mouse Model of Alzheimer's Disease. J Neurosci 26:13384–13389.
Rosario ER, Carroll J, Pike CJ (2010) Testosterone regulation of Alzheimer-like neuropathology in male 3xTg-AD mice involves both estrogen and androgen pathways. Brain Res 1359:281–290.
Rosario ER, Carroll JC, Pike CJ (2012) Evaluation of the effects of testosterone and luteinizing hormone on regulation of β-amyloid in male 3xTg-AD mice. Brain Res 1466:137–145.
Sarkar J, Wakefield S, MacKenzie G, Moss SJ, Maguire J (2011) Neurosteroidogenesis is required for the physiological response to stress: role of neurosteroid-sensitive GABAA receptors. J Neurosci 31:18198–18210.
Seshadri S, Wolf P, Beiser A, Au R, McNulty K, White R, D'Agostino R (1997) Lifetime risk of dementia and Alzheimer's disease. The impact of mortality on risk estimates in the Framingham Study. Neurology 49:498–504.
Sholl DA (1953) Dendritic organization in the neurons of the visual and motor cortices of the cat. J Anat 87(387–406):1.
Singh C, Liu L, Wang JM, Irwin RW, Yao J, Chen S, Henry S, Thompson RF, Brinton RD (2012) Allopregnanolone restores hippocampal-dependent learning and memory and neural progenitor survival in aging 3xTgAD and nonTg mice. Neurobiol Aging 33:1493–1506.
Smale G, Nichols NR, Brady DR, Finch CE, Horton WE (1995) Evidence for apoptotic cell death in Alzheimer's disease. Exp Neurol 133:225–230.
Small SA, Schobel SA, Buxton RB, Witter MP, Barnes CA (2011) A pathophysiological framework of hippocampal dysfunction in ageing and disease. Nat Rev Neurosci 12:585–601.
Smith C, Wekstein D, Markesbery W, Frye C (2006) 3alpha,5alpha-THP: a potential plasma neurosteroid biomarker in Alzheimer's

disease and perhaps non-Alzheimer's dementia. Psychopharmacol 186:481–485.
Taleb O, Patte-Mensah C, Meyer L, Kemmel V, Geoffroy P, Miesch M, Mensah-Nyagan AG (2018) Evidence for effective structure-based neuromodulatory effects of new analogs of neurosteroid allopregnanolone. J Neuroendoc 30.
Wang JM, Singh C, Liu L, Irwin RW, Chen S, Chung EJ, Thompson RF, Brinton RD (2010) Allopregnanolone reverses neurogenic and cognitive deficits in mouse model of Alzheimer's disease. Proc Natl Acad Sci 107:6498–6503.
West MJ, Coleman PD, Flood DG, Troncoso JC (1994) Differences in the Pattern of Hippocampal Neuronal Loss in Normal Aging and Alzheimers-Disease. Lancet 344:769–772.
Yang S, He X (2001) Role of Type 10 17ß-Hydroxysteroid Dehydrogenase in the Pathogenesis of Alzheimer's Disease. Adv Exp Med Biol 487:101–110.
Yassa MA, Stark SM, Bakker A, Albert MS, Gallagher M, Stark CEL (2010) High-resolution structural and functional MRI of hippocampal CA3 and dentate gyrus in patients with amnestic Mild Cognitive Impairment. Neuroimage 51:1242–1252.
Yeap BB, Almeida OP, Hyde Z, Chubb SA, Hankey GJ, Jamrozik K, Flicker L (2008) Higher serum free testosterone is associated with better cognitive function in older men, while total testosterone is not. The Health In Men Study. Clin Endocrinol (Oxf) 68:404–412.
Young HC, Yoo JS, Eun OL, Kayed R, Glabe CG, Tenner AJ (2006) ERK1/2 activation mediates ABeta oligomer-induced neurotoxicity via caspase-3 activation and Tau cleavage in rat organotypic hippocampal slice cultures. J Biol Chem 281:20315–20325.
Zhao L, Yao J, Mao Z, Chen S, Wang Y, Brinton RD (2011) 17β-Estradiol regulates insulin-degrading enzyme expression via an ERβ/PI3-K pathway in hippocampus: Relevance to Alzheimer's prevention. Neurobiol Aging 32:1949–1963.
Zheng H, Xu H, Uljon SN, Gross R, Hardy K, Gaynor J, Lafrancois J, Simpkins J, Refolo LM, Petanceska S, Wang R, Duff K (2002) Modulation of A(beta) peptides by estrogen in mouse models. J Neurochem 80:191–196.
Zhuang S, Schnellmann RG (2006) A death-promoting role for extracellular signal-regulated kinase. J Pharmacol Exp Ther 319:991–997.

(Received 29 August 2019, Accepted 7 January 2020)
(Available online 16 January 2020)